THE NORWEGIAN UNIVERSITY OF SCIENCE AND TECHNOLOGY

PRE-MASTER THESIS

Steering System and Load Case Development in DNV GL Fuel Fighter

Author:
Lars Røed RAMSTAD

Supervisor:
Knut AASLAND, PhD.

Department of Mechanical and Industrial Engineering

Faculty of Engineering

December 12, 2018

THE NORWEGIAN UNIVERSITY OF SCIENCE AND TECHNOLOGY

Abstract

Faculty of Engineering

Department of Mechanical and Industrial Engineering

Steering System and Load Case Development in DNV GL Fuel Fighter

by Lars Røed RAMSTAD

DNV GL Fuel Fighter is a team of students at NTNU, competing at the annual Shell Eco-marathon Europe. The team builds and designs cars that compete in a race against time, but most importantly, a race against fuel consumption.

This pre-master thesis discusses the efforts of the author, and in part other members of the DNV GL Fuel Fighter team in developing a new steering system for the teams 2019 model, as well as developing load cases for the design and dimensioning of the vehicle body and suspension.

A literature review presents a knowledge base on steering systems and some of the factors that affects steering, especially in terms of loss of power. Combined with set competition requirements, this information is used in suggesting and evaluating four steering concepts. Further development of one of the concepts is initiated, and lays the foundation for the continued project work as part of the authors master thesis.

Load cases for braking and turning while driving the car are developed, and measures to assure confidence in these are discussed. Additionally, physical testing is executed with the teams 2018 model, with hopes of being able to predict the loads imposed on the wheels of next years model when driving across angled ramps at speed. Data indicates that it is in fact plausible to make such predictions based on testing, but signal quality proves to be an issue during a large fraction of the tests, and so further work is required.

Acknowledgements

Contents

List of Figures

List of Tables

List of Abbreviations

SEM   Shell Eco-marathon
SEM18 Shell Eco-marathon Europe 2018
SEM19 Shell Eco-marathon Europe 2019
FF   DNV GL Fuel Fighter
FF18   The DNV GL Fuel Fighter 2018 model
FF19   The DNV GL Fuel Fighter 2019 model
cm   Centre of mass
$\mathbf{cm_f}$ Equivalent centre of mass, front axle
$\mathbf{cm_r}$ Equivalent centre of mass, rear axle

List of Symbols

α	Slip angle	°
C_α	Cornering stiffness	N/°
m	Total mass of vehicle	kg
m_f	Equivalent mass, front axle	kg
m_r	Equivalent mass, rear axle	kg
μ	Coefficient of friction, tires on asphalt	N/N
f	Factor of proportionality, normal and frictional load	N/N
g	Standard gravity	9.80665 m/s^2
l	Wheelbase	m
l_f	Horizontal distance, front axle to centre of mass	m
h	Vertical distance, ground to centre of mass	m
w_f	Front axle track-width	m
w_r	Rear axle track-width	m
N_f	Normal load on front wheel	N
N_r	Normal load on rear wheel	N
F_f	Longitudinal frictional load on front wheel	N
F_r	Longitudinal frictional load on rear wheel	N
$N_{o,\,f,r}$	Normal load on outer front or rear wheel	N
$N_{i,\,f,r}$	Normal load on inner front or rear wheel	N
$F_{o,\,f,r}$	Transverse frictional load on outer front or rear wheel	N
$F_{i,\,f,r}$	Transverse frictional load on inner front or rear wheel	N
$N_{o,i\,f}$	Normal load on outer or inner front wheel	N
$N_{o,i\,r}$	Normal load on outer or inner rear wheel	N
$N_{o,\,f}$	Normal load on outer front wheel	N
$N_{i,\,f}$	Normal load on inner front wheel	N
$N_{o,\,r}$	Normal load on outer rear wheel	N
$N_{i,\,r}$	Normal load on inner rear wheel	N
$F_{o,\,f}$	Transverse frictional load on outer front wheel	N
$F_{i,\,f}$	Transverse frictional load on inner front wheel	N
$F_{o,\,r}$	Transverse frictional load on outer rear wheel	N
$F_{i,\,r}$	Transverse frictional load on inner rear wheel	N
l_{sa}	Steering arm length	mm
l_{tr}	Tie rod length	mm
γ_i	Inner wheel steering angle	radians
γ_o	Outer wheel steering angle	radians

β Steering arm angle

Chapter 1

Introduction

1.1 Note to the reader

This pre-master thesis is written independently by a member of the DNV GL Fuel Fighter team. However, much of the work in the DNV GL Fuel Fighter project is done in collaboration between team members. The thesis is written in the passive form, hence, sentences of the form "An analysis was performed..." imply that the analysis was performed by the author himself. In cases where other members have contributed, their names and their contribution is specified.

All text written in red font contains hotlinks, which directs the reader either between different sections of the document, or to external online addresses. Figures 3.4 and 3.5 also contain hotlinks, directing the reader to animated versions of the figures online. The external files that are referenced in these instances are also found in the submission attachment through Inspera.

Many readers prefer low light emission when reading from a screen, to prevent eye fatigue. By default this document is formatted as black text on a white background. However, if preferred for reading comfort, the document is made to support switching to light coloured text on a dark background. (In Adobe Acrobat this is done as illustrated here. It's most effective if also opting for the dark display theme, as instructed here. Hotlinks remain red even as text colour is changed.)

1.2 DNV GL Fuel Fighter and the Shell Eco–marathon

1.2.1 Shell Eco-marathon

The Shell Eco–marathon (SEM) is a series of competitions hosted by Shell. The events allow teams of students from all across the globe to compete on a racetrack using vehicles of their own design. There are three main events; SEM Europe, SEM Americas and SEM Asia, in addition to a series of challenger events leading up to the main regional events.[16] The competition

Figure 1.1: DNV GL Fuel Fighter at the Shell Eco-marathon Europe 2018[15]

hosts three vehicle classes; UrbanConcept, Prototype and Autonomous UrbanConcept (a new vehicle class introduced in 2018). In each vehicle class teams may choose to compete in one of three fuel classes; hydrogen fuel–cell, battery electric and internal combustion engine.[1]

In the UrbanConcept and Prototype classes, drivers are required to finish a set amount of laps around a race track in a set amount of time, while keeping the energy consumption as low as possible. Drivers are required to make a full stop during every lap. The Prototype class focuses on maximum efficiency, while the UrbanConcept class requires a more practical design in order to qualify. During SEM Europe 2018 (SEM18) the race consisted of 15 laps of 970 meters, with a maximum completion time of 35 minutes.[2]

In the Autonomous UrbanConcept class the vehicle is not controlled by a human driver, but by an autonomous system composed of perception sensors and vehicle control systems. Teams compete in navigating through a series of complicated courses. In this case, energy consumption makes up only one out of several metrics when selecting a winner.

1.2.2   DNV GL Fuel Fighter

"DNV GL Fuel Fighter" (FF) is a voluntary student organisation at NTNU, in which students from different programs of study work together to design and build highly fuel efficient road vehicles in order to compete in the annual "Shell Eco–marathon Europe". The team has been competing every year since 2008, securing a spot on the podium on several occasions, while other times not being able to finish the race.[15]

At Shell Eco-marathon Europe 2019 (SEM19), DNV GL Fuel Fighter aims to compete in the UrbanConcept vehicle class, and for the first time; the Autonomous UrbanConcept vehicle class. FF intends to compete in both vehicle classes using the same vehicle, and in both cases compete in the battery electric fuel class.

Organisational Hierarchy

The team consists of five sub-teams; mechanical, electrical, autonomous, design and marketing. Additionally, there is a board consisting of the project administrator, an administrative assistant, the leaders of each sub-team and all students writing their pre-master and/or master thesis based on their FF work. The author of this pre-master thesis is represented in the board and the mechanical sub-team.

1.3 Problem Description and Scope

The vision and mission of DNV GL Fuel Fighter read as follows:

> "Inspire a sustainable future - through learning and creating innovative solutions that challenge today's perception of transportation."

and

> "Develop and build an ultra-efficient UrbanConcept car that excels in Shell Eco-marathon"

Achieving this is a complicated problem, composed of many factors ranging from design and marketing to pure component and systems performance. This technical project work will seek to fulfil the vision and mission by securing the best level of performance possible for the DNV GL Fuel Fighter 2019 model (FF19), while simultaneously attempting to create inspiration and enthusiasm through unconventional solutions.

This pre-master thesis will focus on solving two main challenges; constructing realistic load cases for the dimensioning of the suspension and monocoque chassis of FF19, and designing a new steering system that maximises efficiency while meeting new requirements for the participation in the Autonomous UrbanConcept class.

The importance of well developed load cases lies both in the risk management and performance fields. Ensuring that FF19 is dimensioned to handle realistic loads, and gets through the Shell Eco-marathon in one piece, by simultaneously pushing the safety factors as low as possible to ensure low weight and maximum performance. The load cases will be developed both my means of analytic calculations, as well as physical testing. The physical testing will be performed on the FF18 model, with hopes of being able to utilise the data to predict values for FF19. The load case development is based off of an understanding of mechanical physics, which is assumed known to the reader.

The development of a new steering system contributes towards the mission by attempting to mitigate what was perhaps one of the largest competitive weaknesses of FF18, while simultaneously attempting to inspire new and out

of the box thinking, in light of the vision statement. The development of a new steering system will include the entire process from product requirements, early ideas, prototype design and testing, up until the current state of the development. The steering system development is based off of theoretical knowledge of steering systems presented in the literature review (2.1), as well as requirements set by the Shell Eco-marathon and the DNV GL Fuel Fighter team (3.1).

At first glance these two parts of the pre-master thesis do not seem particularly closely related. However, the intention is for steering system development to be tied closer together with front suspension development in the following semester, in which the load cases are of absolute relevance. Thus, solving both these problems is necessary for the intended master thesis that is to follow from this pre-master work. This project work only reflects the first half of a larger project, and therefore the final design, production and testing of the steering system, in addition to the actual application of the load cases developed are outside its scope.

Chapter 2

Literature Review

2.1 Steering Systems

The objective of a steering system is to enable the vehicle to travel along an arc, thus rotating around a turn centre and altering the direction of travel. Steering a vehicle is a process that causes inherent mechanical losses. In an energy consumption challenge such as SEM it is therefore of utmost importance to minimise those losses.

2.1.1 Ackermann Steering

Traditionally, horse drawn carriages utilised a steering system in which both front wheels were fixed to a common axle. and that axle was free to rotate around a pivot point at its centre. This system had the advantage of both front wheels being on the same axis, and so the axis of all four wheels would always intersect in the turn centre. The axle was pivoted by the horse(s), as it was directly drawn. However, this system posed challenges for use in automotive vehicles, as the driver was required to apply large forces in order to turn the entire axle. [3, pg.305]
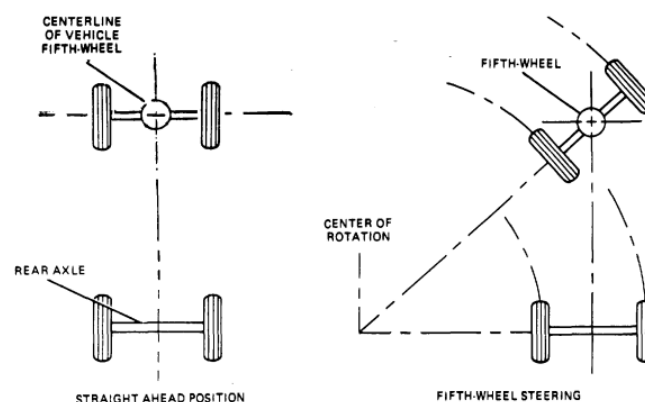
Figure 2.1: Fith–wheel steering[4, fig.33-2]

A solution to this problem was developed in 1817, namely the Ackermann Steering system.[3, pg.305] The front wheel axis is fixed, however both front

wheels are attached to a spindle that may rotate around a kingpin. Steering arms are attached to the spindles (together composing the "steering knuckle"), and a tie rod connects them. The steering arms are attached at an angle, thus the assembly forms a trapezoid. This ensures that the inner wheel rotates further around its kingpin than the outer wheel, given a certain sideways shift of the tie rod. This is referred to as a toe-out turn, as the wheels are pointed slightly apart as opposed to being parallel.[5, pg.541]

The intention is for all axis of all wheels to intersect in a common turn centre. This is called "perfect Ackermann steering", however, the Ackermann system itself is only an approximation and not in reality able to achieve this ideal geometry.
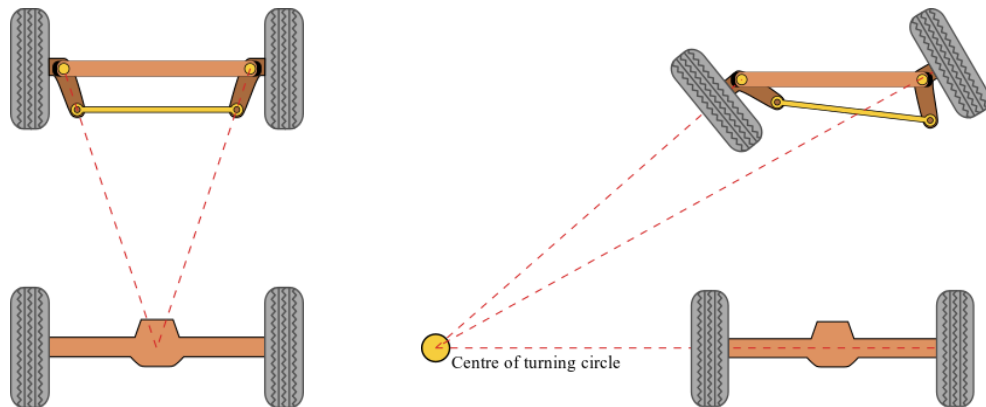
Figure 2.2: Ackerkmann steering when driving in a straight line
and when turning.[17]

Nearly all cars on the market today utilise some adaption of the Ackermann system, however there are a number of ways it may be actualised.

Parallelogram Systems

In a parallelogram system a centre link connects the tie rods from each wheel. The centre link is attached to two arms, the Pitman arm and the idler arm. Rotating the Pitman arm forces the centre link to shift side to side, thus steering the wheels. The Pitman arm is attached to the sector shaft, which is again driven by the steering column shaft (connected to the steering wheel, thus being the driver input). The geared linkage between the steering column shaft and the sector shaft is named the steering box, and may be configured in a number of ways, e.g. with a worm and sector gear, worm and roller or through the recirculating ball system. The recirculating ball system is similar to a worm and sector gear, except the worm is made up of a shaft covered in bearing balls, greatly reducing the friction and thus driver effort required to turn the steering wheel. The recirculating ball system is therefore commonplace in large and heavy vehicles.[3, pg.308]
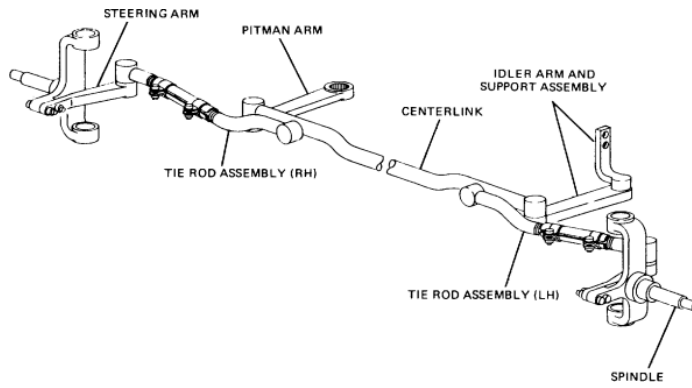
Figure 2.3: Parallelogram steering.[4, fig.33-5]
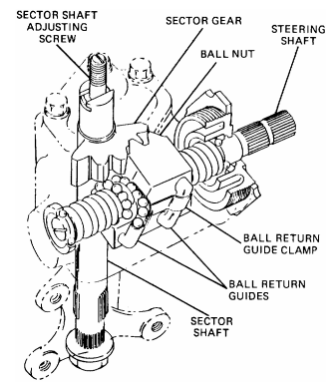
Figure 2.4: Recirculating ball.[4, fig.33-10]

Rack and Pinion

In the rack and pinion system the centre link is mounted on a fixed path, free to move along one axis only. A tooth rack is attached directly on top of the centre link, which is in turn driven by a pinion on the steering column shaft. Rotation of the pinion directly shifts the centre link from side to side, thus rotating the wheels around the kingpins through the tie rods. The rack and pinion system is simple and lightweight, in addition to providing feedback to the driver (the driver can feel forces applied to the wheels through the steering wheel), thus it is commonly found in small vehicles and sports cars.[3, pg.308]
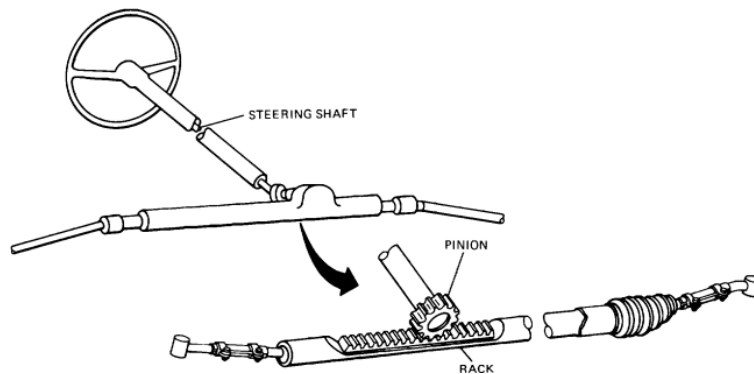
Figure 2.5: Rack and pinion steering[4, fig.33-11]

2.1.2   Steer by Wire

In spite of its efforts, the Ackermann system is not able to cause all wheel axis to intersect the common turn centre perfectly with varying turning radii. In addition to this, there are certain deviations at speed which means it is not necessarily optimal to achieve perfect Ackermann geometry, these are discussed in 2.2. As a solution to this, vehicle manufacturers are likely to adapt adaptive electronic steering systems in the near future, referred to as "steer

by wire" systems. By allowing each front wheel to be controlled individually by electronic actuators, the vehicle control unit can provide the optimal steering angle for each wheel based on desired turning radius as well as current load, speed and tire properties. Steer by wire systems can potentially increase energy efficiency, improve handling capabilities and improve safety, both trough the enhanced handling capabilities and the absence of the steering column shaft, which is a dangerous object to have in front of the driver during a collision.[6, pg.513-526]

2.2 Slip Angles

When turning at speed, the tires are subject to lateral forces, providing the centripetal acceleration of the vehicle. In generating these forces the tires experience some deformation, causing *slip angles*. The slip angle is the angular deviation between a wheels orientation and its direction of travel. The relationship between a wheels cornering force and slip angle may be considered linear for slip angles smaller than $5°$.[3, pg.312][7]

$$F_y = C_\alpha \alpha \tag{2.1}$$

The factor of proportionality, C_α, is the cornering stiffness, and is dependant on tire properties and load. As will be seen in 4.2.2, the loads on the outer wheels are larger than on the inner wheels during a turn, thus the slip angle is not equal across wheels. This is especially true for high speed and small turning radii. Adaptions in the steering geometry are often made to compensate for this, adaptions in which the engineers aim for significantly less toe-out than with perfect Ackermann geometry are called anti-Ackermann steering, and is common in racing cars.[8]

2.2.1 Effect on Tire Drag

The 2005 winning SEM Prototype team PAC-car II[9] performed the following analysis to determine the effect of slip angles on tire drag when turning.

For a given tire, the cornering stiffness was approximated by a simplified version of Pacejka's "magic formula" model[9, pg.59][10]:

$$C_\alpha = (a_{30} + a_{31}P)sin\left(2tan^{-1}\left(\frac{F_z}{a_{40} + a_{41}P}\right)\right) \tag{2.2}$$

The coefficients were given for the tire in question, and the tire pressure was set at 6 bar, making the cornering stiffness a function of vertical load only.

The simplest way to observe tire slip is through the "unicycle model", i.e. assuming a single wheel rolling around a turn centre in steady state.

The steady state assumption defines the following equilibrium:

$$F_y cos\alpha - F_x sin\alpha = mv^2/R \tag{2.3}$$

$$F_y sin\alpha + F_x cos\alpha = T \tag{2.4}$$

Equation 2.4 illustrates how the traction T provided to the wheel must compensate for the tire drag to maintain steady state. The F_x component of the tire drag represents the longitudinal component of rolling resistance in the tires/wheels, while the F_y component represents the transverse component of the cornering force. A larger slip angle results in a larger longitudinal component of cornering force, and thus large slip angles increase tire drag.

Assuming $\alpha < 5°$, equation 2.1 holds, while $cos\alpha \approx 1$, and $sin\alpha \approx \alpha\frac{\pi}{180}$ (where the slip angle α is expressed in degrees.)

Introducing this in 2.3 and 2.4 we get:

$$\alpha = (\frac{mv^2}{2})/(C_\alpha - F_x) \tag{2.5}$$

$$T = C_\alpha\alpha^2\frac{\pi}{180} + F_x \tag{2.6}$$

From 2.6 and 2.5, the tire drag at different turning radii and velocities, are plotted in figure 2.7, assuming a given vehicle mass and associated rolling resistance. The aerodynamic drag of PAC-car II is plotted alongside the tire drag, illustrating that the tire drag is of a significant magnitude in comparison. Bear in mind that the unicycle model produces higher slip angles than if the load was distributed on four wheels. As the tire drag is proportional with the slip angle squared, the actual tire drag may not be as high in a four wheel model.

However, when moving from the unicycle model to a full vehicle model, the slip angles can be "forced" higher than necessary if the steering angle
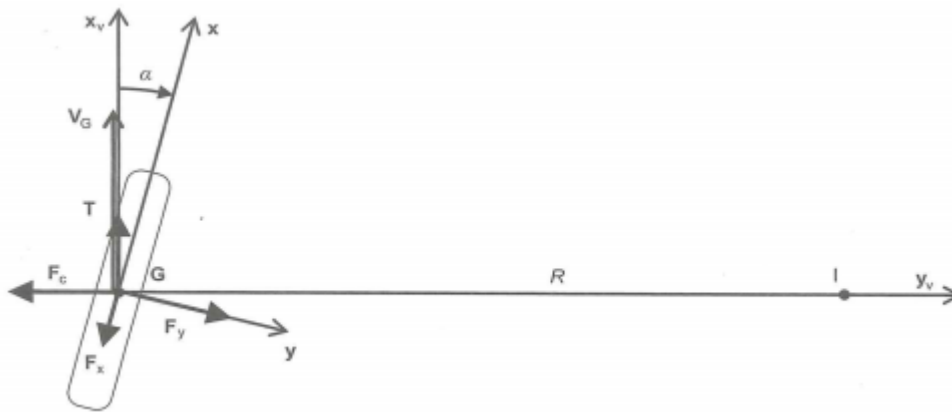
Figure 2.6: Free body diagram of the "unicycle model".[9, pg.74]
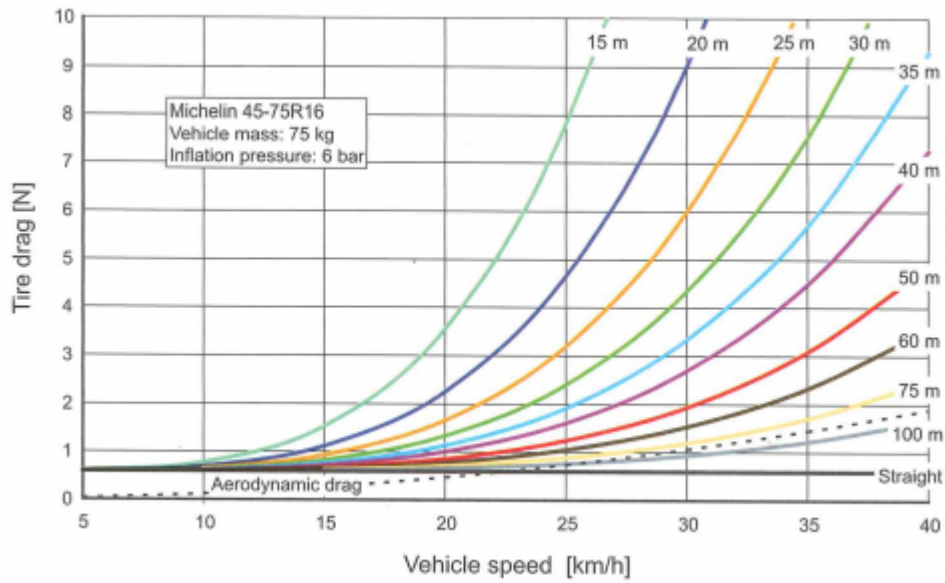
Figure 2.7: Effects of speed and turning radius on tire drag.

relationship between the wheels is not ideal. As we have seen, high slip angles has a significant effect on tire drag, and therefore, designing a steering system than can provide ideal steering geometry should be made a priority when efficiency is of the highest importance.

Chapter 3

Steering System Development

3.1 Requirements

3.1.1 Regulatory Requirements

ARTICLE 47: TURNING RADIUS AND STEERING

a) Vehicle steering must be achieved by one system operated with both hands using a turning motion. It must be precise, with no play or delay. Steering must be operated predominately through the front wheels.

b) Steering must be achieved using a steering wheel or sections of a wheel with a minimum diameter of 250 mm.

c) Steering bars, tillers, joysticks, indirect or electric systems are not permitted.

d) The turning radius must be 6 m or less. The turning radius is the distance between the centre of the circle and the external wheel of the vehicle. The external wheel of the vehicle must be able to follow a 90°arc of 6 m radius in both directions. The steering system must be designed to prevent any contact between tyre and body or chassis.

e) The Organisers reserve the right to set up a vehicle handling course to verify the following when the vehicle is in motion: driver skills, turning radius and steering precision.

-Shell Eco-marathon 2019 Official Rules[1, pg.21]

Seen are the steering system requirements set by Shell for the 2019 Eco-marathon. Note particularly that the rules do not allow the use of electric steering systems, such as the steer by wire systems discussed in 2.1.2. The requirement of achieving a turning radius of 6 meters or less defines the required maximum steering angle for a given set of vehicle dimensions. The requirement of

avoiding contact between tyres and vehicle body in turn defines the required wheel well dimensions.

3.1.2 Design Requirements

In addition to the requirements set by Shell, there are a number of internal requirements and constraints to be met when designing a steering system.

Physical Design Space

Figure 3.1b displays a cross section of FF19, with a driver, illustrating how the legs of the driver consume space between the front wheels. Shell Eco-marathon 2019 Official Rules states:

> Article 30 a)
>
> *It is imperative for Drivers, fully harnessed, to be able to vacate their vehicles at any time without assistance in less than 10 seconds.*[1, pg.16]

With this in mind it was made a priority for the steering system to avoid being excessively intrusive of the space occupied by the driver when operating and entering/exiting the vehicle.

Figure 3.1a displays another cross section of the chassis. Notice how the floor of the body curves up between the wheel wells and the centre of the drivers compartment. A traditional steering system usually occupies the space in a direct line between the hubs of the two front wheels, which in this case involves penetrating through the chassis in the curved sections. However, in light of article 46 b) in the official rules, this is not an option for FF19.

> Article 46 b)
>
> *The vehicle body must cover all mechanical parts when viewed from all sides. The wheels and suspension must be fully covered by the body when seen from above, and the wheels must be covered up to the axle centre line when seen from front or rear. The covering for the wheels and suspension must be a rigid, integral part of the vehicle body.*[1, pg.21]
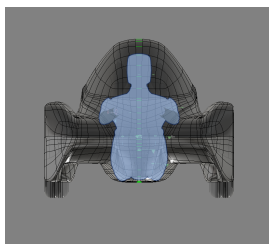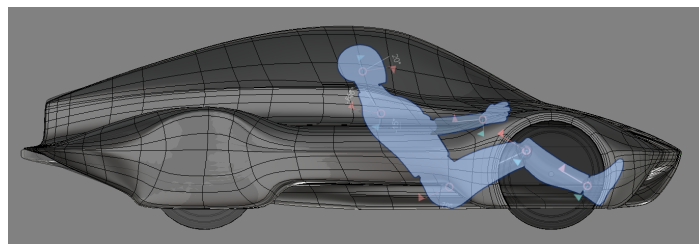
| (a) Front view | (b) Side view |

Figure 3.1: Cross section views of the drivers position in vehicle cabin.

In addition to these factors, a dashboard and a braking system that will be installed in the drivers compartment are not displayed in the figures, and contribute to further limiting the space available for steering design.

Autonomous Operation

In order to compete in the Autonomous UrbanConcept class, the steering system must be operable without driver input, i.e. with the use of electronic actuators.

This involves making the necessary space and mounts for the actuator, and ensuring that the operation of the steering does not require a too high amount of power. If the steering becomes very power demanding, this will impact both the electrical power consumption directly, as well as indirectly, following the need of a large and powerful actuator.

Steering Geometry

As discussed in 2.1, an efficient steering system requires a different steering angle on each wheel, to ensure that the transverse tire forces do not have an unnecessarily large component opposite of the direction of movement. The widely used Ackermann system attempts to accomplish this, although it never reaches "perfect Ackermann geometry". Additionally, as noted in 2.2, "perfect Ackermann" is not necessarily preferred. Steer by wire systems are able to accommodate any desired combination of steering angles, however, as illustrated in 3.1.1, these are not allowed in competition.

Therefore, there was a desire for the design of a mechanical system that allowed itself to be calibrated to any desired combination of steering angles. This turned out to be a highly consuming priority in the following design process.

3.2 Initial Idea Phase

3.2.1 Creating an Overview

The idea phase started with only the most conspicuous requirement in mind – the system needs to translate the turning motion of the steering wheel into the turning motion of the two front wheels. Thus began a review of every motion translation device palpable. These were divided into two categories:

- Those initiated in the contact patch of two mediums
    - Spur and helical gears
    - Bevel and worm gears

  - Lead screws

  - Levers and links

  - Pulleys

  - Rails/guides

  - Flexible couplings

- Those conducted through a medium over a distance

  - Wires

  - Shafts

  - Flexible shafts

  - Hydraulic tubes

  - Chains

  - Belts

Some of these devices immediately stood out, both in a negative and positive fashion. E.g. bevel and worm gears produce high amounts of friction[11, pg.714], which increases the power required for autonomous operation (the exception to this being recirculating ball type worm gears, as discussed in 2.1.1). Wire and hydraulic systems, on the other hand, were seen in a positive light, as they can easily translate motion between completely different locations and orientations, thus allowing the designer to limit the use of space in crowded locations in the drivers cabin.

In order to achieve different steering angles for each wheel with a given angle of the steering wheel, there needs to be a none-constant translation ratio between components. Traditional gears can not achieve this without changing the gears, while e.g. rails and guides, belt and wire pulleys and chain sprockets are able to do this continuously by varying their shape. Alternatively, as in the Ackermann system, sets of levers and links can also achieve non-constant translation ratios. One might also considered that worm gears or lead screws could produce variable translation ratios by varying the thread pitch along their length. However, it is not obvious how such a component may be produced.

3.2.2   Brainstorming

Based on the overview presented in 3.2.1, sets of ideas were conceptualised and sketched. Figure 3.2 illustrates an idea to extend the steering column shaft from the steering wheel all the way to a steering box in the nose of the vehicle, where space is more plentiful, allowing wires or hydraulics to translate the motions rearwards to the wheels. Detailed in this sub-section are the concepts that received the most attention, some of which are based off of the idea illustrated in figure 3.2.
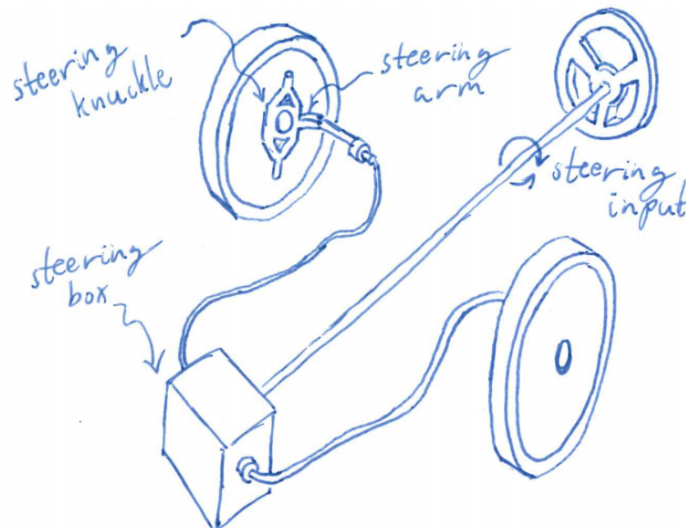
Figure 3.2: Extended steering column shaft

Hydraulic Screw Piston

The steering column shaft drives a screw into an hydraulic cylinder. This concept could be used in one of two ways; a single hydraulic screw piston could drive a traditional Ackermann system centre link side to side; or, by fabricating two sets of screws and pistons with variable thread pitch one could allow individual angling of each wheel as desired. A major part of the idea was for the pistons to be transparent, and clearly visible in the drivers cabin, thus making them a design feature.

Uneven Wire Pulleys

This concept based itself off of an idea by project administrator Eirik Furuholmen. A double set of unevenly shaped pulleys attached to the steering column shaft drives wires that turn the wheels individually. The shape of the pulleys define the translation ratios and thus the steering geometry.

Double-Guide Wheel

The double-guide wheel system consists of a wheel attached to the steering column shaft, in which two grooves are made. Each groove guides a linear piston in or out when the steering wheel is turned. From there, each of the linear pistons drives either wires or hydraulics or "tie-rods" (see 2.1.1) to the steering arms of each of the front wheels. The radial distance from the centre of the double-guide wheel to the groove at any given angle defines the steering angle of the wheel it controls.
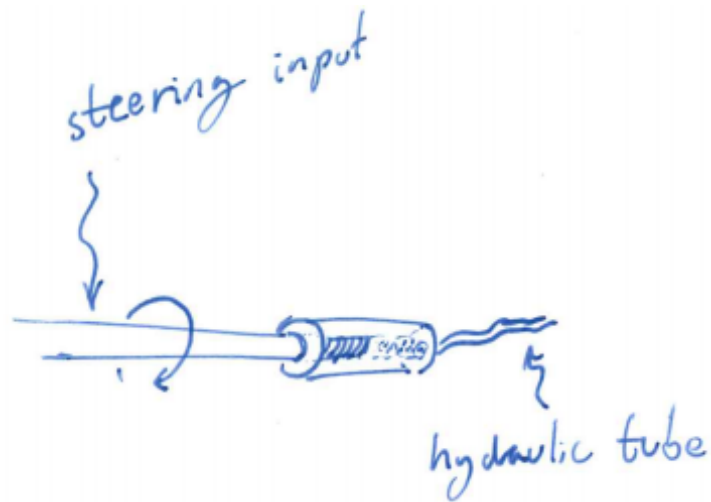
(a) Hydraulic screw piston
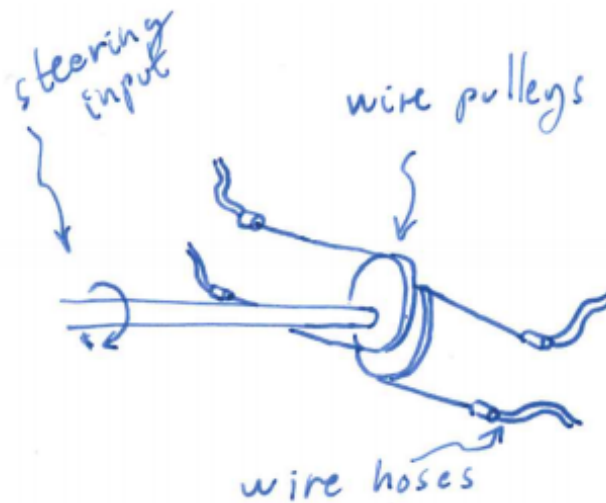
(b) Uneven wire pulleys
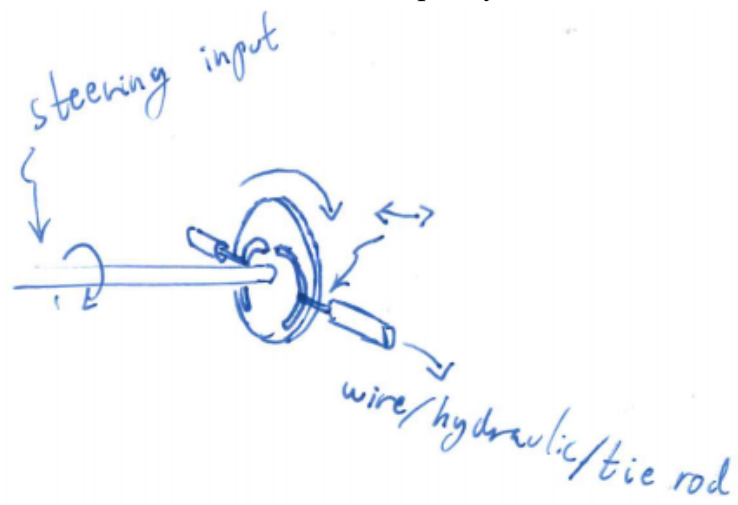
(c) Double-guide wheel

Figure 3.3: Plausible steering concepts.

Rack and Pinion

In addition to developing these new concepts, the rack and pinion steering system used in FF18 was assessed for possible reuse. In FF18, the rack and pinion was floor-mounted between the two front wheels. However, as seen in 3.1a, use of this space is limited. The steering arm of the steering knuckle in the suspension system can theoretically be extended vertically to any height within the rim of the wheel. Looking at 3.1b, there appears to be space between the wheels in what represents the first quadrant of the wheel circle in that view, over the drivers ankles. Hence, if extending the steering arm vertically to that position, the rack and pinion could be mounted from the top down, in stead of on the floor. This will also serve the advantage of not interfering with the braking pedal and cylinder layout. This positioning will require the driver to pull his/her legs out from underneath the centre link of the steering system when exiting the vehicle, hence it does complicate the fulfilment of Article 30 a)[1, pg.16], discussed in 3.1.2.

3.3 Concept Elimination

There was insufficient capacity within the team to enter into detailed design of all four concepts. However, inspired by set-based design principles[12], there was also reluctance towards simply choosing the most attractive concept and continue development. In stead, the concepts were subject to two iterations of consideration, in order to eliminate concepts from the bottom up.

3.3.1 Requirement Fulfilment

Use of Space

The four concepts were evaluated based on their ability to fulfil the requirements discussed in 3.1. In terms of use of space, the uneven wire pulley system, and the double-guide wheel systems scored highly, as they could be positioned anywhere and translate motion to the wheels through wires or hydraulics. The hydraulic screw piston system had the same advantage, given the second of the two proposed configurations, in which there are two pistons, one for each wheel. The first configuration of the hydraulic screw piston and the rack and pinion system from FF18 both suffered the disadvantage of requiring space in-between the wheels.

Power Demand

Considering the use of electronic actuators to power the steering, the concepts were evaluated in terms of assumed power demand. The uneven wire

pulley concept was assumed to be operable with low power, and experience
dictated the same for the rack and pinion system. The hydraulic screw pis-
ton concept on the other hand fell short, as threaded connections are known
to produce a high amounts of friction, especially under pressure.[11, pg.714]
To reduce the friction, the radius of the piston would need to be large, re-
quiring more space, and resulting in higher weight. Scepticism existed as to
whether the double-guide wheel system could operate smoothly, and so a
decision was made to create a simple implementation prototype[13, pg.376]
to validate the concept.

Figure 3.4: Implementation prototype of double-guide wheel
concept. (click the figure or caption to see a motion animation)

A model was created in CAD, consisting of a frame, a wheel with carved
out guides, and two pistons with pins that glide along the guides. The as-
sumption being that if a small-scale simple FDM prototype with poor sur-
face finish, loose tolerances and pins that glide along the guides could op-
erate smoothly, then so would a full scale, smoothed component with guide
rollers. The results were in fact validating. A model showed surprisingly
smooth operation at first attempt.

Steering Geometry and Re-Calibration

Finally, the degree to which the concepts could provide ideal steering geom-
etry and re-calibration was assessed. The rack and pinion concept works by
the Ackermann steering design, and is known to only approximate the per-
fect Ackermann steering geometry. The steering geometry can be adjusted by
changing the length and angle of the steering arms, and re-calibrated if these
parts are made adjustable. In the case of the existing system from FF18, they
were not. The uneven wire pulley concept and the double-guide wheel con-
cept both allow the designer to achieve the exact desired steering geometry.
Furthermore, the geometry is in both cases defined by as single component
only, the pulley/wheel, and so the steering geometry can be completely re-
defined by changing only a single component. Finally, the hydraulic screw
piston could potentially utilise the geometry of the rack and pinion system,
or define its own. But in the latter case, both the two pistons and their screws

would need to be redesigned and manufactured in order to re-calibrate the steering geometry.

First Elimination

Based on the first round of assessment, the hydraulic screw-piston appeared to be the weak link. Not only did it not deliver well in terms of the set requirements, but additionally it appeared unnecessarily complicated, with no apparent advantage over the other concept. Except perhaps for the prospect of being utilised as a design feature. Subsequently, the concept was eliminated.

3.3.2 Feasibility

Rack and Pinion

The three remaining concepts were evaluated in terms of how easily they could be designed, manufactured and assembled in FF19. The rack and pinion system from FF19 was of course already designed and manufactured. As described in 3.2.2, based on CAD models there appeared to be sufficient space to mount the system in FF19, though it would likely be a sub-optimal fit.

Double-Guide Wheel

The double-guide wheel concept was assessed to be easily designed and manufactured. The steering angle of each wheel is determined by the radius of the groove at any angle of the steering wheel. Simple trigonometry is all that is required to go from a desired steering angle relationship and the design of the steering groove. Manufacturing of the wheel could be CNC-milled with a regular three-axis machine, and the pistons could be bought from a supplier.

Uneven Wire Pulley

Determining the shape of the uneven wire pulley to produce a desired set of steering angle ratios is more computationally demanding. The point of tangent between the wires and the pulleys move as the pulleys rotate when they are of an uneven shape, thus, not only does one need to consider the radius at any angle, but also the accumulated path-length along the pulley up until the moving tangent point. However, once designed the pulleys themselves could possibly easily be manufactured in a three-axis CNC-mill.

Second Elimination

The assessment concluded that the rack and pinion system from FF18 served strong advantages by already being built and proven functional. An adaption of the existing system for FF19 would therefore be a low risk solution demanding low effort. The double-guide wheel served strong advantages in being able to work with either wires, hydraulics or tie-rods, providing full control of steering geometry, and not necessarily demanding use of space between the wheels. The uneven-pulley system promised nearly the same, with the exception of excluding the possibility of using hydraulics or tie-rods. The combination of being more complicated to design and showing no other apparent major advantages led to the uneven pulley concept being shelved.

3.3.3   Decision

Based on the findings a strategy was selected; to continue development on the double-guide wheel concept, while adapting the old rack and pinion system for installation in FF19 as a fail safe. The major piece of justification for not fully abandoning the rack and pinion system was risk mitigation. Even though the rack and pinion system from FF18 is by no means optimal, it is proven functional. Starting development of a brand new concept is always a risk in itself, with a wast amount of unknowns. Attempts were made to search for similar applications of the mechanism used in the double-guide wheel concept online, with no success. Thus, attempting to design an unproven concept under time pressure, with no back-up solution was considered reckless. After all, in a competition like the Shell Eco-marathon, a barely working design on time is better than an optimal solution one day late.

3.4   Further Development

3.4.1   Concept Improvement

In addition to concept validation, the implementation prototype discussed in 3.3.1 revealed several opportunities for improvement. One being that in the case of wires or hydraulics being used to transfer motion, both pistons could be mounted on the same side, making the wheel two-sided. This would make the system more area compact, and mounting both pistons together could possibly save weight. Additionally, it allows each guide to utilise all 360° of the wheel, thus increasing the range of rotation of the steering wheel, and reducing the required power to drive the mechanism. Figure 3.5 illustrates the concept with this adaption.

Additionally, a realisation was made that the guides could rather be made out of "ridges" with rollers on each side, in stead of grooves with rollers inside. This would make the wheel itself much thinner, and thereby save

weight, in addition to removing the issue of making the rollers compact enough to fit inside the grooves.

Figure 3.5: CAD assembly of improved double-guide wheel concept. (click the figure or caption to see a motion animation)

3.4.2 Integration Prototype

In order to further validate and improve the concept, testing is needed. Therefore design was initiated on an integration prototype[13, pg.377] for FF18, so that it might be used in testing while FF19 is being built. The following criteria were set:

- Allow a 6 m outside wheel turning radius, in accordance with SEM requirements.[1, pg.21]

- Maintain a linear relationship between the turning angle of the steering wheel, and the steering angle of the inner wheel.

- the system should be compatible with the tie rods and steering knuckles already mounted in FF18.

The linear movement of the pistons required to produce a given steering angle was determined through simple trigonometry. The same goes for the steering angles for any steering radius, assuming perfect Ackermann steering. These relationships allowed us to determine the radius of the guide in the double-guide wheel at every angle.

The absolute dimensions of the double-guide wheel mechanism is somewhat arbitrary, a larger wheel results in a lower guide radius gradient, and in turn smoother operation. The size needed for satisfactory operation needs to be determined by experience. For the purpose of this prototype, a 20 cm outer diameter was selected, this leaves a bare minimum of space between the guide and the centre of the guide-wheel at the smallest radius. To be compatible with the use of tie-rods, the concept improvement illustrated in figure 3.5 was not utilised. Thus, less than 180° of the wheel is available to each guide, meaning the 6 m turn radius must be achieved within 90° rotation of the steering wheel.

Figure 3.6: Steering angles in the "perfect Ackermann" steering geometry.

$$\gamma_i = tan^{-1}\left(\frac{l}{\sqrt{R^2 - l^2} - w_f}\right) \tag{3.1}$$

$$\gamma_o = tan^{-1}\left(\frac{l}{\sqrt{R^2 - l^2}}\right) \tag{3.2}$$

(a) Driving straight

(b) Turning

Figure 3.7: Relationship between piston movement x and steering angle γ in FF18 (steering knuckle in green, steering arm in yellow, piston in blue)

$$x = l_{tr}\left[1 - cos\left(sin^{-1}\left(l_{sa}\frac{[cos(\beta) - cos(\beta + \gamma)]}{l_{tr}}\right)\right)\right] - l_{sa}\left[sin(\beta + \gamma) - sin(\beta)\right] \tag{3.3}$$

Designed was initiated in Autodesk Inventor Professional, using polar function curve features. There are two symmetrical guides, one controlling each wheel. Each guide consists of two halves, one half controls the steering when the guides wheel is on the inside of the corner, and the other when the wheel is on the outside of the corner. The first half of the curve is controlled by equation 3.3, where γ is substituted by γ_i. In the other half of the curve γ is substituted by γ_o as function of γ_i. Thus, at any angle of the steering wheel the system provides different steering angles to each wheel, coherent with perfect Ackermann steering geometry.
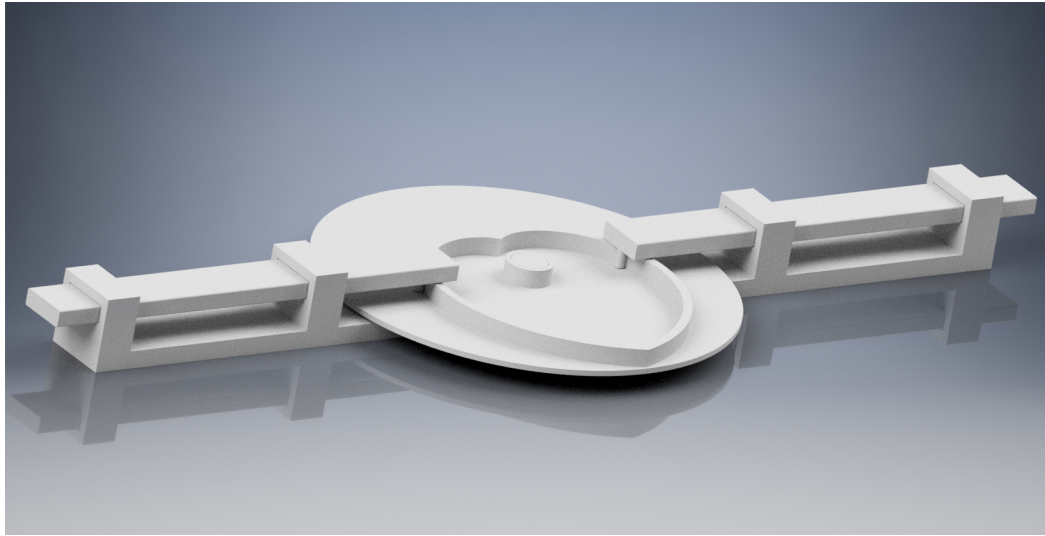
(a) Assembled view
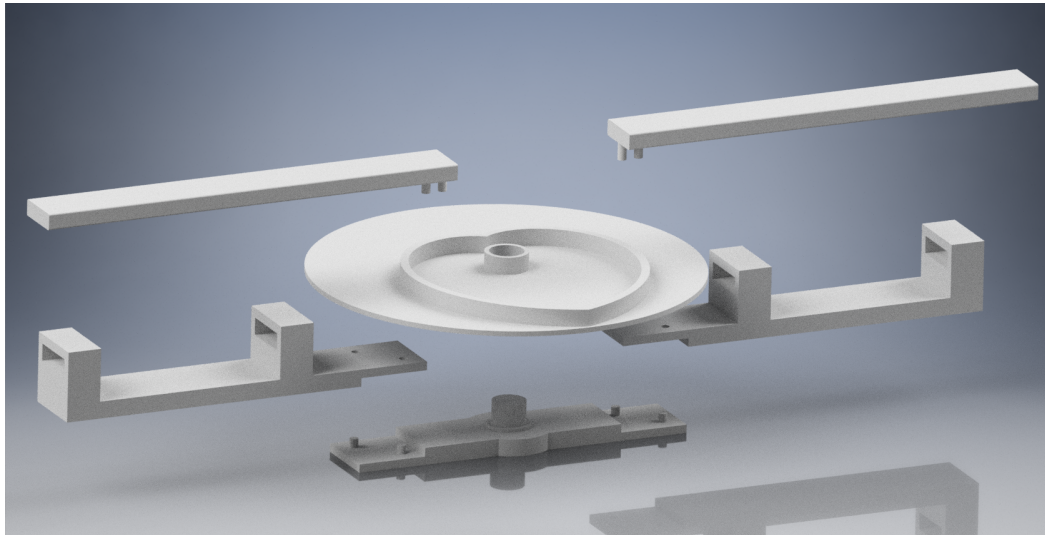
(b) Exploded view

Figure 3.8: Integration prototype CAD design.

At the time of this pre-master submission, the integration prototype is close to being ready for production and initial testing using FF18. Continuing this work is the number one point on the agenda for the continuation of this project.

Chapter 4

Load Case Development

4.1 Identifying the Necessary Load Cases

In order to dimension the suspension system and the vehicle body properly, knowledge is required as to what loads the vehicle might be subject to in operation. This includes both the relevant loads when driving the vehicle, as well as lifting, towing, entering/exiting and so forth. In addition to this, there are set requirements in SEM for tolerating loads applied to the roof of the vehicle, and the drivers safety belt.[1, pg.15]

In this thesis we'll examine the external loads on the vehicle when driving. Three scenarios that induce loads on a vehicle in operation have been examined:

- Braking

- Turning

- Driving across an uneven surface

The first two have been examined by analytical calculations, while the third was examined through physical experiments with the FF18 vehicle.

4.2 Analytical Calculation

4.2.1 Braking

Article 51 in the Shell Eco-marathon 2019 Official Rules[1, pg.23] sets strict requirements for the braking system in the vehicle. A four-disc hydraulic brake system operated by a single pedal, controlling one or two master cylinders is required. Additionally, it is required for the system to operate independently on the front and rear axis, or in an X pattern (left front with right rear and vice versa). In the following calculations, independent operation on the front and rear axles is assumed. This is the most logical assumption, due to such a system being more easily mounted. The assumption also allows us to further

assume that the braking power on the left and right side of each axle is equal, thus simplifying the calculation to a 2D problem.

As the rules require a powerful braking system, we further assume that the braking system in FF19, once built, will be powerful enough such that the maximum limitation on braking power is defined by tire to road surface friction. As the maximum coefficient of friction is that of static friction[18], the maximum braking power case is that in which the wheels experience pure rolling, and the brakes are approaching the limit of locking up.
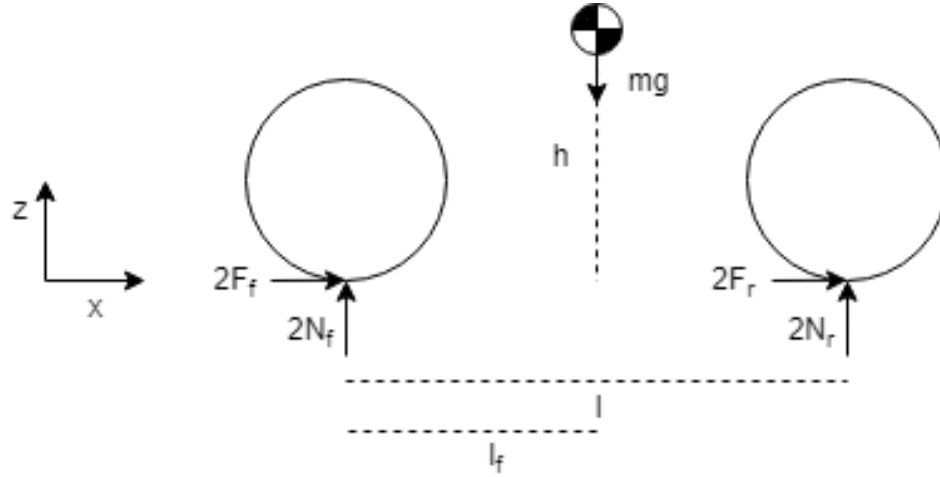
Figure 4.1: Braking load schematic

Figure 4.1 illustrates the 2D simplified calculation model for braking loads. The direction of movement is in the negative x-direction, while the direction of the braking acceleration is in the positive x-direction. Each wheel drawn illustrates two wheels in the depth axis. l represents the wheelbase, l_f represents the horizontal distance from the front axle to the vehicles centre of mass, and h represents the vertical distance from the road surface to the vehicles centre of mass. N_f, F_f, N_b and F_b represents the normal and frictional loads on each wheel in the front and rear-end of the vehicle.

We define the three equilibrium equations:

$$\sum F_x = F_{braking} = 2(F_r + F_f) = ma \tag{4.1}$$

$$\sum F_z = 0 = mg - 2(N_r + N_f) \tag{4.2}$$

$$\sum M_{y,cm} = 0 = 2N_f l_f - 2N_r(l - l_f) - 2(F_r + F_f)h \tag{4.3}$$

Maximum Power Braking on all Four Wheels

Assuming maximum braking power on all four wheels we get:
$F_f = N_f \mu$ and $F_r = N_r \mu$.

Combining this with equations 4.2 and 4.3 results in:

$$0 = 2(\frac{mg}{2} - N_r)l_f - 2N_r(l - l_f) - 2(N_r + \frac{mg}{2} - N_r)\mu h \tag{4.4}$$

Which yields:

$$N_r = \frac{mg(l_f - \mu h)}{2l} \tag{4.5}$$

$$N_f = \frac{mg(l - l_f + \mu h)}{2l} \tag{4.6}$$

$$F_r = \frac{mg(l_f - \mu h)}{2l}\mu \tag{4.7}$$

$$F_f = \frac{mg(l - l_f + \mu h)}{2l}\mu \tag{4.8}$$

Maximum Power Braking on the Front Wheels Only

Assuming maximum braking power on the front wheels only we get:
$F_f = N_f\mu$ and $F_r = 0$.

Combining this with equations 4.2 and 4.3 results in:

$$0 = 2N_fl_f - 2(\frac{mg}{2} - N_f)(l - l_f) - 2N_f\mu h \tag{4.9}$$

Which yields:

$$N_r = \frac{mg(l_f - \mu h)}{2(l - \mu h)} \tag{4.10}$$

$$N_f = \frac{mg(l - l_f)}{2(l - \mu h)} \tag{4.11}$$

$$F_r = 0 \tag{4.12}$$

$$F_f = \frac{mg(l - l_f)}{2(l - \mu h)}\mu \tag{4.13}$$

Maximum Power Braking on the Rear Wheels Only

Assuming maximum braking power on the rear wheels only we get:
$F_f = 0$ and $F_r = N_r\mu$.

Combining this with equations 4.2 and 4.3 results in:

$$0 = 2(\frac{mg}{2} - N_r)l_f - 2N_r(l - l_f) - 2N_r\mu h \tag{4.14}$$

Which yields:

$$N_r = \frac{mgl_f}{2(l + \mu h)} \tag{4.15}$$

$$N_f = \frac{mg(l - l_f + \mu h)}{2(l + \mu h)} \tag{4.16}$$

$$F_r = \frac{mgl_f}{2(l + \mu h)}\mu \tag{4.17}$$

$$F_f = 0 \tag{4.18}$$

Example loads

The exact dimensions and mass distribution of FF19 are not yet known, as the vehicle is still in development. Using a set of assumed values we can calculate the loads on the vehicle when braking. These are used in the first iteration of dimensioning the vehicle body and suspension. The results of the dimensioning provides the mass distribution for the next iteration, and so forth.

m [kg]	l [m]	l_f [m]	h [m]	μ
150	1.7	0.7	0.4	0.72

(a) Example parameters (mass and dimensions provided by Eirik Furuholmen, friction coefficient determined in appendix A)

Braking on	N_f	N_r	F_f	F_r
All wheels	557	178	401	128
Front wheels	521	215	375	0
Rear wheels	477	259	0	186

(b) Resulting loads

Table 4.1: Example of braking loads. [N]

We see that when using these example parameters the maximum vertical and frictional load on the front wheels occur during braking on all four wheels. The maximum vertical and frictional loads on the rear wheels occur when

braking on the rear wheels only (note also that the vertical loads on the rear wheels is always lower than $mg\frac{l_f}{l}$, thus lower than the vertical loads on the rear wheels during standstill/free rolling). Braking on the front wheels only does not result in any worst case scenarios, and so this load case becomes irrelevant in dimensioning.

4.2.2 Turning

In 2.2.1 we calculated the turning loads using the "unicycle model". Among other well known models that exists for this purpose we find the "bicycle model" and "tricycle model"[9, pg.79]. However, in a full vehicle model with four wheels, the problem becomes under-determined. Solving such a system becomes more difficult, as suspension and body stiffness becomes a factor. The body itself is not yet fully developed, and neither is the suspension. Therefore we depend on making valuable assumptions to be able to develop turning load cases.

When developing load cases for dimensioning purposes it is usually the worst case scenarios that interest us the most, therefore we'll consider high speed turning. Experience dictates that the maximum speed held at SEM is approximately 30 km/h.[14, pg.83] High speed turns rarely occur at the smallest turning radii, and so we are assuming that the turning radius is sufficiently large such that the centripetal acceleration may be considered constant and uni-directional throughout the vehicle. The cornering stiffness of our tires is not currently known. Despite tire slip being a major influence in efficiency, tire drag forces are not of a magnitude that makes them relevant in dimensioning. Therefore we ignore the effects of tire slip and rolling resistance.

We construct a new model where we ignore the torsional stiffness of the vehicle body. The front and rear wheel axles can now twist and turn independently of each other, making the problem determined. This scenario is of course not fully realistic; in FF19 the suspension stiffness will likely be much higher in the front than in the rear.

When turning, the softer rear suspension will have to travel a certain distance for the rear outer wheel to develop enough vertical forces to achieve a moment equilibrium around the longitudinal axis of the vehicle. The front outer wheel on the other hand can produce these loads with less suspension travel, and the vehicle body's torsional stiffness can prevent the rear end of the vehicle from tilting further. Thus the front outer wheel takes up a higher load to achieve moment equilibrium than if the front and rear axles can tilt independently.

To compensate for this uncertainty, we also utilise the tricycle vehicle model. In this model, the front wheels produce all the moment that keeps the vehicle from rolling. Thus we know that in the real world case, the vertical loads on
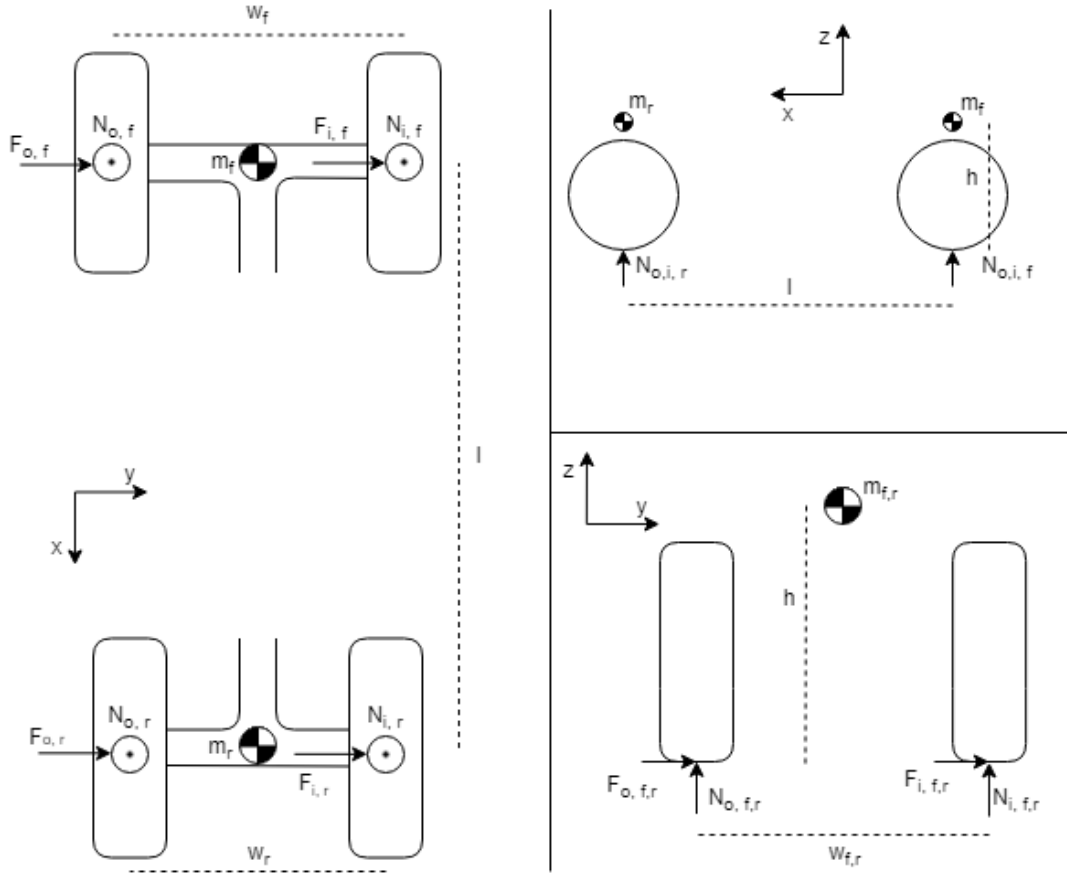
Figure 4.2: Top-, side- and rear view of the independent axle
model

the outer front wheel lies somewhere in-between that of the independent axle
model and the tricycle model.

Independent Axle Model

At SEM18, the tightest turn radius on the track was approximately 17 m.
Driving through a 17 m radius turn with $l = 1.7\ m$ only requires a steering
angle of less than $6°$ when assuming no tire slip. For ease of calculation
we choose to neglect this angle, thus the model appears as a vehicle driving
straight, but with a transverse acceleration of v^2/r.

We find the fraction of the mass held through the front and rear axles:

$$m_f = \frac{l - l_f}{l}m, \ m_r = \frac{l_f}{l}m \tag{4.19}$$

And establish the equilibrium equations for the two axles:

$$\sum F_z = N_{o,\,f,r} + N_{i,\,f,r} = m_{f,r}g \tag{4.20}$$

$$\sum M_{x,cm} = 0 = (N_{i,\,f,r} - N_{o,\,f,r})w_{f,r}/2 + (F_{o,\,f,r} + F_{i,\,f,r})h \tag{4.21}$$

Assuming that the frictional load on a given tire is proportional with its normal load, through the factor of proportionality f, where $f = \frac{v^2/r}{g}$ (provided the factor does not exceed μ), we get:

$$N_{o,\,f,r} = m_{f,r}g(1/2 + fh/w_{f,r}) \tag{4.22}$$

$$N_{i,\,f,r} = m_{f,r}g(1/2 - fh/w_{f,r}) \tag{4.23}$$

$$F_{o,\,f,r} = m_{f,r}g(1/2 + fh/w_{f,r})f \tag{4.24}$$

$$F_{i,\,f,r} = m_{f,r}g(1/2 - fh/w_{f,r})f \tag{4.25}$$

Solving these equations with the same parameters as seen in 4.1a, front and rear axle width of $w_f = 1.2\ m$ and $w_r = 1.0\ m$ (also provided by Eirik Furuholmen), and an assumed velocity and turning radius of $v = 30\ km/h$ and $r = 17\ m$, we get the loads seen in table 4.2.

$N_{o,f}$	$N_{i,f}$	$N_{o,r}$	$N_{i,r}$	$F_{o,f}$	$F_{i,f}$	$F_{o,r}$	$F_{i,r}$
553	313	404	202	230	130	168	84

Table 4.2: Resulting loads [N] using the independent axle model.

Tricycle Model

With only three wheels the model becomes determined, and there is only need for one set of equilibrium equations:

$$\sum F_z = N_{o,\,f} + N_{i,\,f} + N_r = mg \tag{4.26}$$

$$\sum M_{x,cm} = 0 = (N_{i,\,f} - N_{o,\,f})w_f/2 + (F_{o\,f} + F_{i,f} + F_r)h \tag{4.27}$$

$$\sum M_{y,cm} = 0 = (N_{i,\,f} + N_{o,\,f})l_f - N_r(l - l_f) \tag{4.28}$$

Keeping the assumption of friction proportional to normal load from the independent axle model, equations 4.26 and 4.28 yield:

$$N_{i,\,f} + N_{o,\,f} = mg\frac{l - l_f}{l} \tag{4.29}$$

and
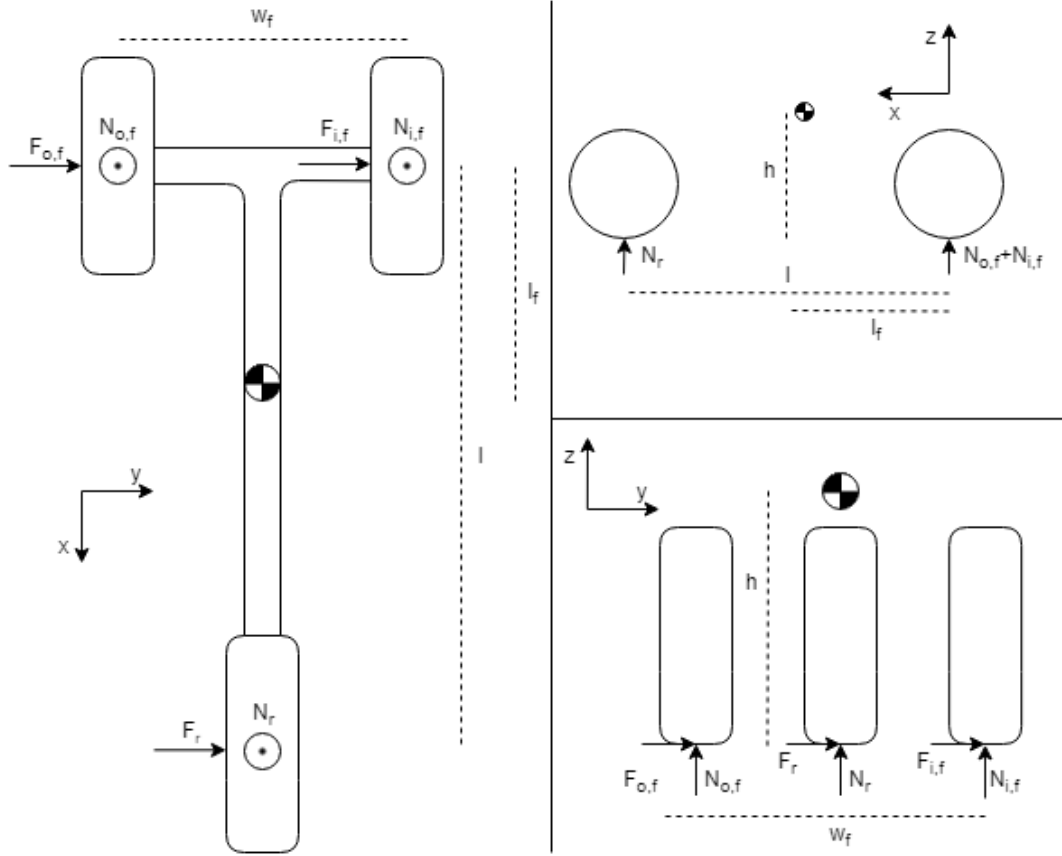
$$N_r = mg\frac{l_f}{l} \tag{4.30}$$

Figure 4.3: Top-, side-, and rear view of the tricycle model

Combining this with equation 4.27 we get:

$$N_{o, f} = mg \left(\frac{(l - l_f)}{2l} + \frac{fh}{w_f} \right) \tag{4.31}$$

$$N_{i, f} = mg \left(\frac{(l - l_f)}{2l} - \frac{fh}{w_f} \right) \tag{4.32}$$

and

$$F_{o, f} = mg \left(\frac{(l - l_f)}{2l} + \frac{fh}{w_f} \right) f \tag{4.33}$$

$$F_{i, f} = mg \left(\frac{(l - l_f)}{2l} - \frac{fh}{w_f} \right) f \tag{4.34}$$

$$F_r = mg \frac{l_f}{l} f \tag{4.35}$$

The resulting loads using the same parameters as in the independent axle model are seen in figure 4.3. Note that the rear wheel loads are exaggerated compared to a real world four wheel scenario, the purpose of using the tricycle model is to examine the effect on the outer front wheel only.

$N_{o,f}$	$N_{i,f}$	N_r	$F_{o,f}$	$F_{i,f}$	F_r
637	228	606	265	95	252

Table 4.3: Resulting loads [N] using tricycle model.

4.3 Physical Testing

4.3.1 Test Design

In order to assess realistic values of the loads imposed on the vehicle body when driving across an uneven surface, physical testing was utilised. The experience of team members taking part in previous years Shell Eco-marathon was that the tracks in general are quite even. Observing video material from SEM17 revealed that ramps had been utilised between track sections and across cable bundles on some sections of the track. Thus, a decision was made to build a ramp that measures the force load imposed on itself when being run over.

The ramp was designed in CAD, and built as a welded steel frame. The top surface of the ramp consists of a large steel plate, hinged to the frame on one end, and resting on an "AEP C8S"[19] load cell borrowed from the Department of Structural Engineering on the other end. The distance from the hinges to the load cell is known, and the load on the load cell is measured during testing. By measuring the distance from the hinges to the point at which the wheels impact the test ramp when diving across it, the load on the wheels is determined through moment equality about the hinges.
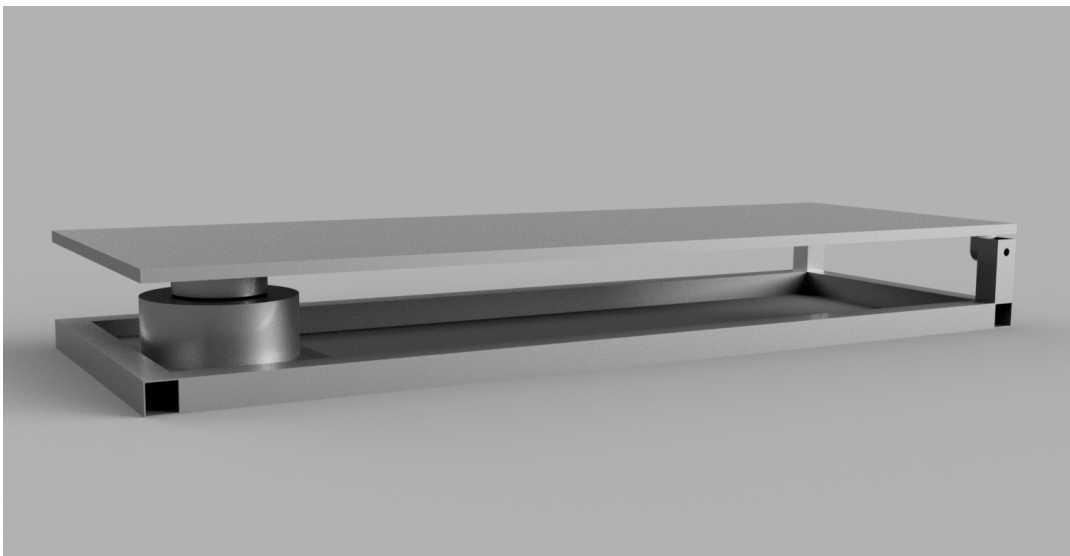

Figure 4.4: CAD design of load testing ramp with load cell.

The objective was to drive across the ramp a number of times with FF18, varying the speed, the inclination angle of the ramp and the mass distribution of the vehicle. The hope was that this would allow relationships to be discovered, between the speed, inclination and distribution of load on each axle when static. The latter factor would allow us to extrapolate the results, so that they could be used to predict values for FF19, with its different mass distribution.

4.3.2   Set-Up and Test Completion

In order to roll onto the approximately 10 cm tall load testing ramp the surface surrounding it needed to be lifted. Six collapsible tables were used, in addition to four large wooden ramps to roll on to and off of the tables, and one small wooden ramp to roll off of the load testing ramp. Team member Sarah Prescott aided significantly in designing and constructing this set-up.

The ramps were set-up on an asphalted section covered by a roof ("Perleporten"). The C8S load cell was connected to an "HBM QuantumX"[20] data acquisition system, from which electrical team leader Haavard Fiskaa recorded the data. Team members Jennifer Nguyen and Robin Solheim acted as test drivers. A total of 19 tests were run, across two days of testing, using four different levels of test ramp inclination, three different mass distributions and a number of speeds.

4.3.3   Results

Noise

Detailed information and data readings from every test is given in appendix B. The first day of testing provided clear data readings, however, the second day of testing was affected by significant levels of signal noise obscuring the data. In some cases the noise reached such a level that it is difficult to interpret what part of the signal represents the impacts. Hence, tests 2.1, 2.2, 2.7, 3.1, 3.2, 3.3 and 3.4 were removed from the analysis. With all of the tests using the third mass distribution removed, the remaining tests make for a quite slim data basis. It is at this point not yet clear what caused this sudden increase in noise, however it is being investigated by Haavard Fiskaa, in hopes of being able to rectify the problem in order to run further tests next semester.

Compiling Results

The test data was grouped in order of the mass distributions and the front and rear wheel loads independently. For each group, resulting maximal impact loads calculated from the data readings are plotted against speed and

ramp inclination. After the removal of the most noise impacted tests, this results in four three-dimensional plots.

Figure 4.5 shows clear trends, in which increased speed and ramp inclination results in increased load imposed on the wheels. The loads are somewhat higher on the front wheel compared to the rear wheel, as is also expected, as the static load on the rear wheel is lower, and so is the suspension stiffness. An attempt by Eirik Furuholmen to use the data for load prediction is presented in appendix C.

Figure 4.6 on the other hand, shows no clear trends. These measurements are from test day 2, at which the noise level was much higher. This may have impacted the precision of the results. Without satisfactory data from test day two, relationships between the changing mass distribution and resulting loads can not be determined. FF19 will have a different mass distribution than FF18, thus, being able to observe such relationships is an absolute necessity for the further use of this data, in order to make the data relevant for the dimensioning of FF19.

4.4 Confidence

A number of uncertainties are always present when attempting to assess real world operating conditions. Higher confidence in the applicability means lower safety factors can be applied in dimensioning. In the case of the braking load cases, they depend on the assumption that load is evenly distributed from one side to the other. The turning load cases recognise that there is a risk of underestimating the loads on the outer front wheel, and thus implements the tricycle model to find an upper limit, increasing confidence in the results. The loads resulting from either braking, turning or driving over a ramp have been assessed, however, in the real world there is always a risk of these cases occurring simultaneously. The effect of combined load cases is not simply a matter of adding the loads. E.g. in the case of braking while turning, the increased loads on the outer wheels from turning also increases the frictional loads from braking. To take these effects into account, one must be meticulous about selecting the right constraints and load applications in the FEM analysis software. However, that is outside the scope of this premaster thesis.

The physical tests assume that the major factors influencing the ramp loads are the ramp inclination, speed and mass distribution of the vehicle. Suspension stiffness, on the other hand is not part of the analysis. As the suspension system for FF19 is not yet designed some assumptions have been made, namely that the rear suspension stiffness in FF19 will be similar to that of FF18. On the other hand, the front suspension in FF19 is currently set to be designed as a rigid suspension with no spring or dampener. To emulate
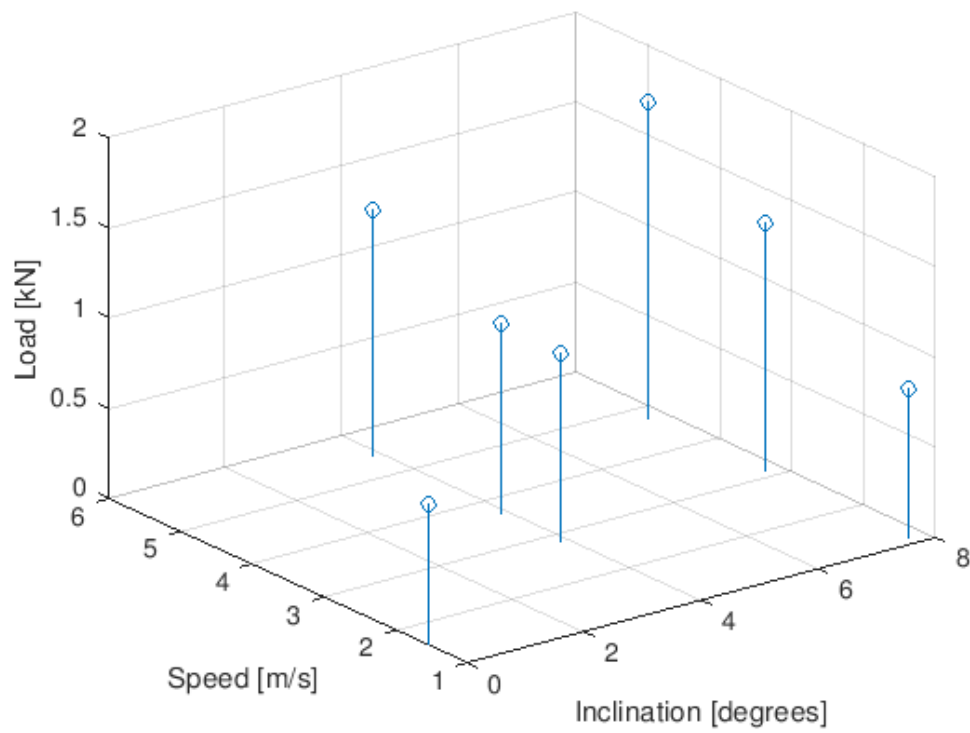
(a) Front wheel
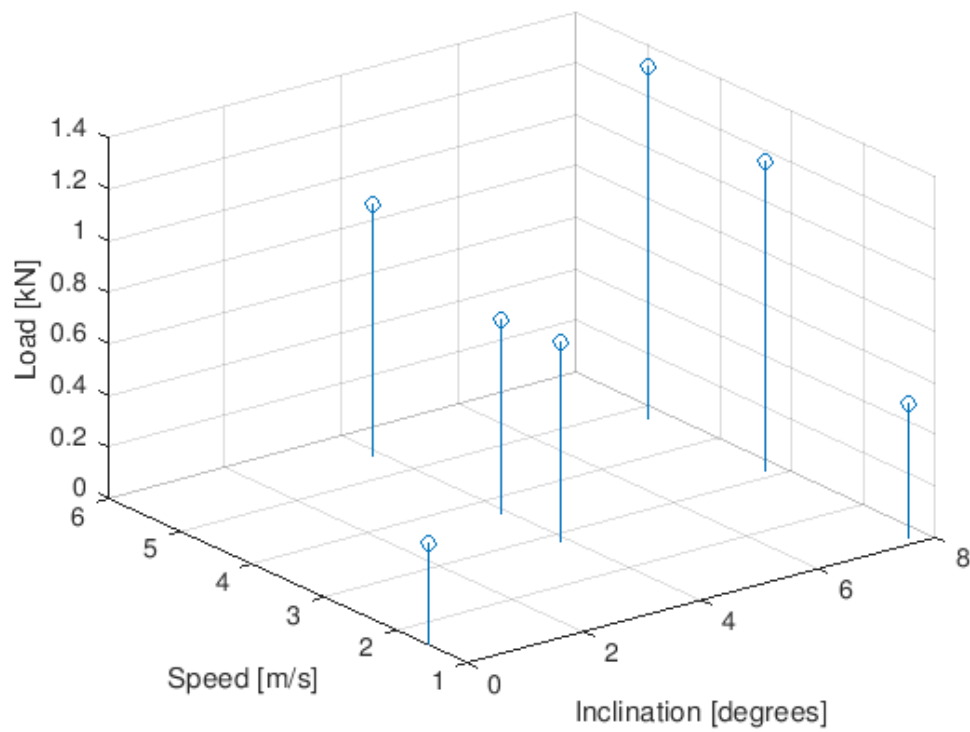
(b) Rear wheel

Figure 4.5: Loads from first mass distribution, plotted against
ramp inclination angle and vehicle speed.
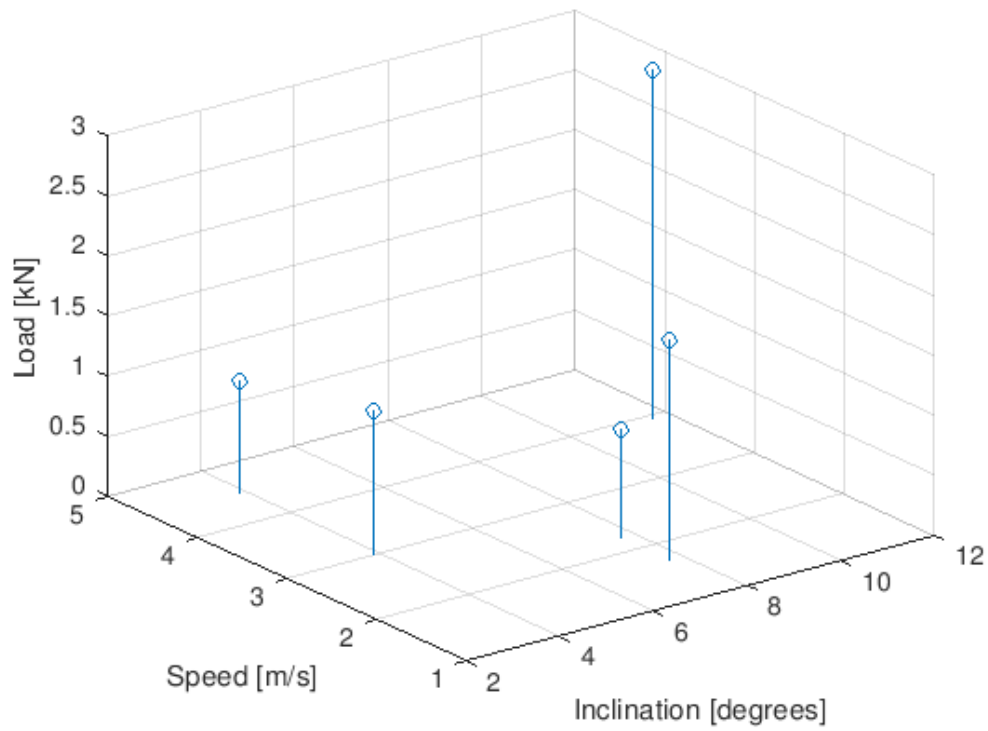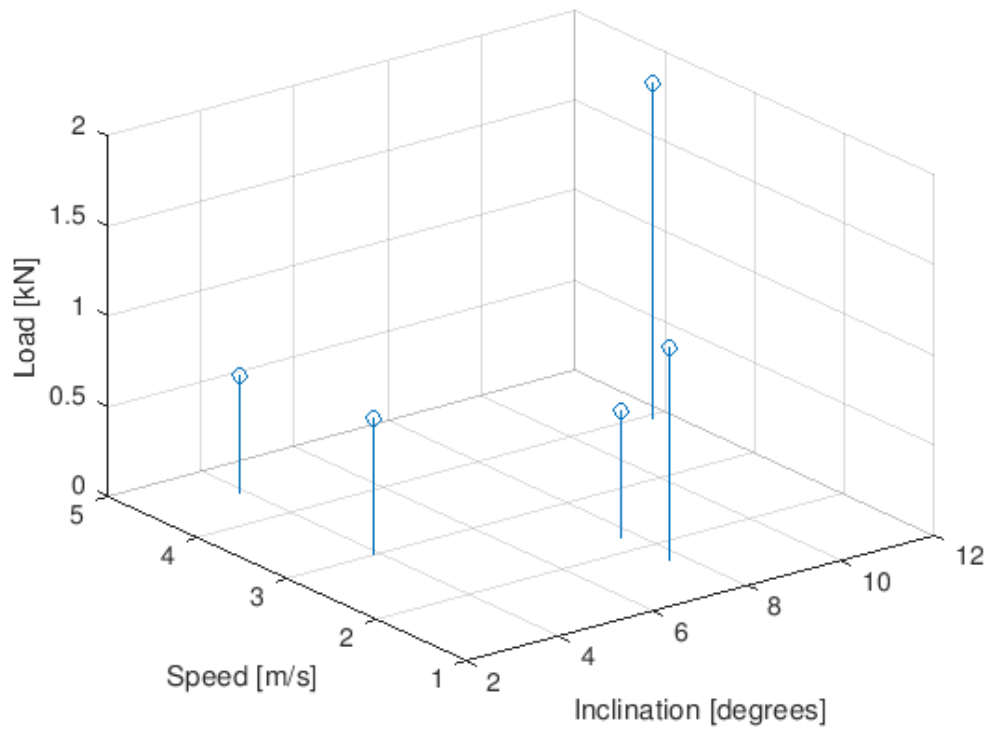
(a) Front wheel

(b) Rear wheel

Figure 4.6: Loads from second mass distribution, plotted against ramp inclination angle and vehicle speed.

these conditions, the front suspension dampeners of FF18 were set to maximal stiffness during testing. Though, some compliance must be assumed, and should therefore motivate increased safety factors.

Chapter 5

Conclusions and Moving Forward

5.1 Steering System

As part of this project work, several new steering system concept have been proposed and evaluated, and to some extent tested. The mathematical foundation for designing and building the double-guide wheel steering concept with perfect Ackermann steering geometry has been made. In the upcoming master work, it is intended for this foundation to be utilised in the testing and further development of this concept. Additionally, there is a desire to design tests that will determine the optimal steering geometry for the purposes of FF19 in SEM 19, which will include the effects of slip angles and other dynamic effects. Ultimately, this will hopefully result in the design and production of a system that aids DNV GL Fuel Fighter in its mission to excel at the Shell Eco-marathon.

5.2 Load Cases

The work detailed in this pre-master thesis provides the ability to properly dimension FF19 to be able to withstand relevant applications of braking and turning at speed. Additionally, the physical testing that has been performed so far indicates that it is in fact possible to obtain physical test data that allows us to predict impact loads when driving across a ramp at an angle. Further testing is necessary to increase both the quantity and quality of available data before this analysis can be put to use.

5.3 Future Work

This project is by no means at its end. In the semester that awaits an entire car is to be built. It is intended for the master thesis that serves as a successor to this work to discuss both the final development of the steering system, as well as being able to apply the work laid down in developing the load cases. Front suspension design and development is set to be a topic, thus

tying the two parts of this pre-master work together, by utilising the load cases in dimensioning while at the same time designing for compatibility with the steering system. Presumably, the master work will also include a higher degree of cooperation with other team members, as the suspension is designed in accordance with vehicle body and braking system as well.

Appendix A

Determining Friction Coefficient of Tires

For purposes of load case development, determining the friction coefficient of the tires was required. The tires are of the type Michelin UC 95/80R16, and are utilised at the maximum rated pressure of 5 Bar.

The two front wheels were attached to the ends of a square section of steel bar. A threaded bar was fed through the centre of the steel bar, at the bottom end of the threaded section, a 10 kg weight plate was attached.

The entire assembly was weighed five times using a simple digital luggage scale. Then the assembly was placed on asphalted pavement, and attempted pulled horizontally five times, using the same luggage scale to measure the loads. The maximum load recorded before the tires started slipping was noted.

The luggage scale read the load in kilograms, as the equivalent load under standard gravity. As the coefficient of friction is unit-less, this does not effect the calculation, which is defined by the ratio of maximum transverse load and normal load.

	Normal load	Transverse load	Friction coefficient μ
	18.9	12.7	
	19.2	13.9	
	19.1	13.8	
	19.2	15.4	
	19.3	13.5	
Average	19.1	13.9	0.72

Table A.1: Measured loads [kg] and resulting friction coefficient.

Appendix B

Load Testing Data

B.1 Test Set-Up Data

| Test	Static load on front wheels	Static load on rear wheels	Ramp inclination	Speed	Front wheel impact distance	Rear wheel impact distance
1.1	423 N	305 N	0.0 °	1.5 m/s	0.38 m	0.53 m
1.2	423 N	305 N	3.8 °	3.7 m/s	0.46 m	0.59 m
1.3	423 N	305 N	3.8 °	2.8 m/s	0.37 m	0.50 m
1.4	423 N	305 N	3.8 °	5.4 m/s	0.35 m	0.48 m
1.5	423 N	305 N	7.7 °	1.1 m/s	0.42 m	0.55 m
1.6	423 N	305 N	7.7 °	3.1 m/s	0.35 m	0.48 m
1.7	423 N	305 N	7.7 °	4.7 m/s	0.39 m	0.53 m
2.1	418 N	295 N	0.0 °	n/a	0.44 m	0.56 m
2.2	418 N	295 N	0.0 °	n/a	0.33 m	0.47 m
2.3	418 N	295 N	3.8 °	3.0 m/s	0.24 m	0.38 m
2.4	418 N	295 N	3.8 °	4.5 m/s	0.30 m	0.43 m
2.5	418 N	295 N	7.7 °	1.7 m/s	0.28 m	0.41 m
2.6	418 N	295 N	7.7 °	2.2 m/s	0.33 m	0.47 m
2.7	418 N	295 N	11 °	n/a	0.23 m	0.39 m
2.8	418 N	295 N	11 °	3.9 m/s	0.24 m	0.37 m
3.1	405 N	414 N	11 °	n/a	0.44 m	0.59 m
3.2	405 N	414 N	11 °	n/a	0.35 m	0.50 m
3.3	405 N	414 N	7.7 °	n/a	0.40 m	0.54 m
3.4	405 N	414 N	3.8 °	n/a	0.34 m	0.49 m

Table B.1: Data regarding the set-up and execution of each test.

For each of the three load distributions, the car was weighed using bathroom scales. The load on the front and rear wheels are reflected in table B.1. The speed at each test is determined as the ratio between FF18's wheelbase of 1.52 m, and the length of the time interval between the two impact peaks

seen from the load data. Thus, it can not be determined for the most noise affected tests. The distance from the load ramps hinges to the point of impact of the front and rear wheels was measured by observing the tire tracks on the ramp. To make the tracks visible the top plate was covered with chalk between each test.

B.2 Load Cell Data

The data from the load cell is logged as .txt documents, in which each row contains the time in seconds and load in kN. The files are available here. Figure B.1 contains plots of all the tests. Note: tests 1.3, 1.4, 1.6 and 1.7 show a third impact shortly before or after the two major impacts. This is the result of team members running across the ramps.
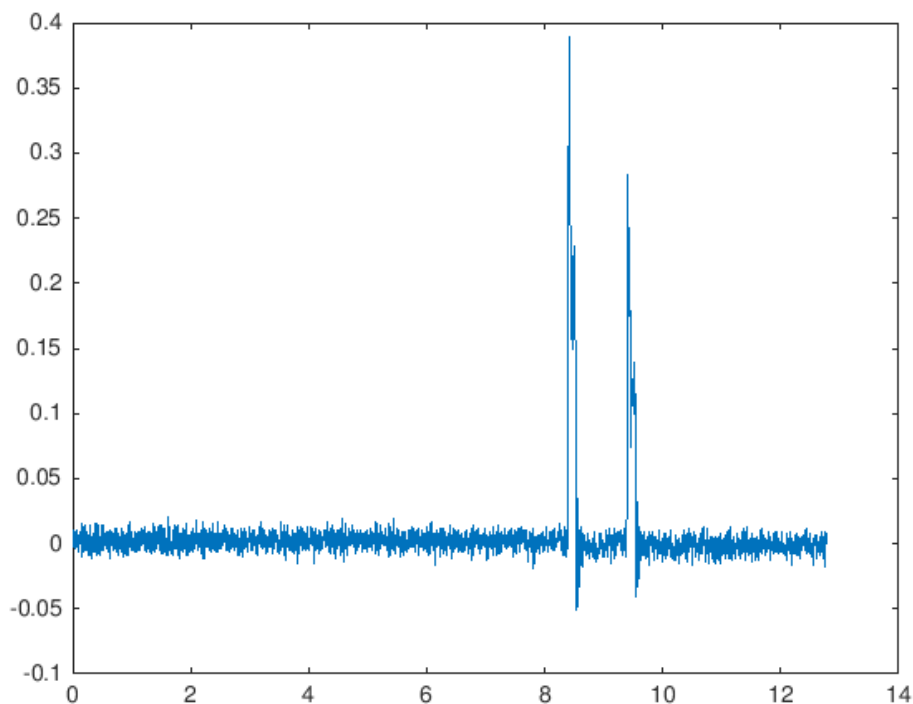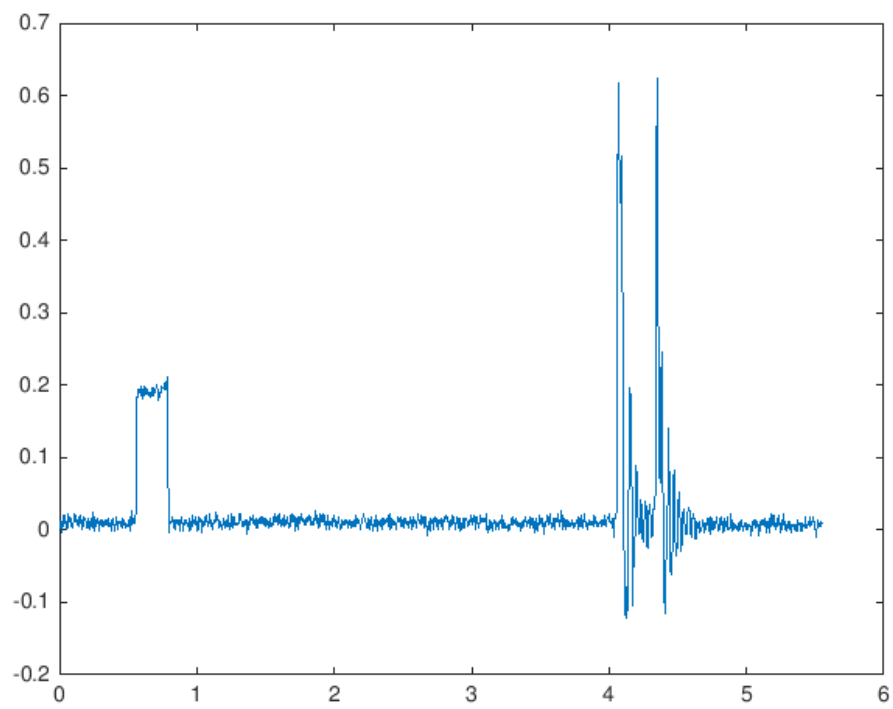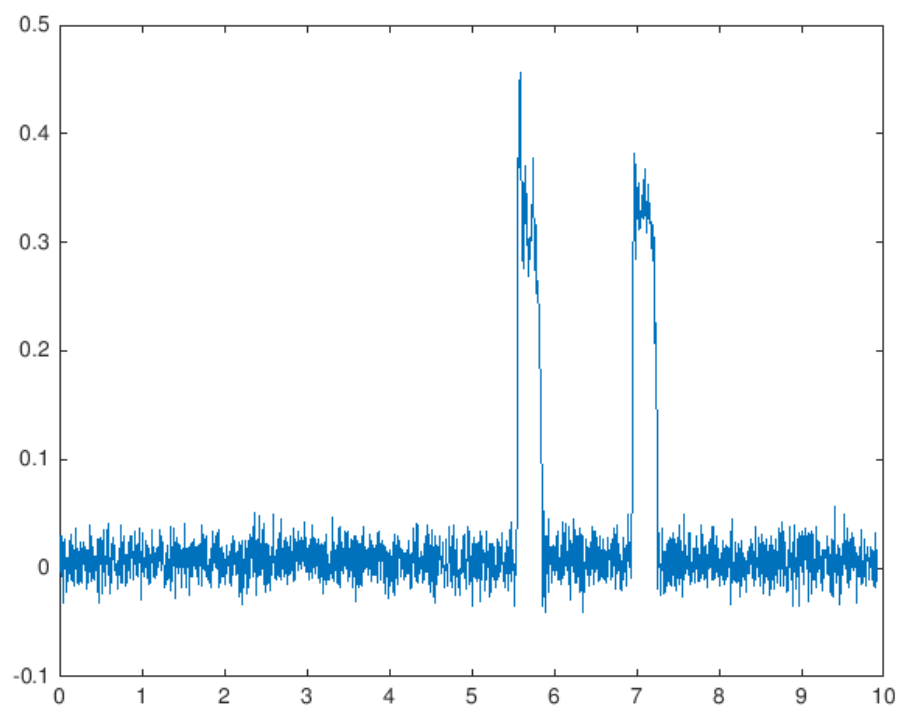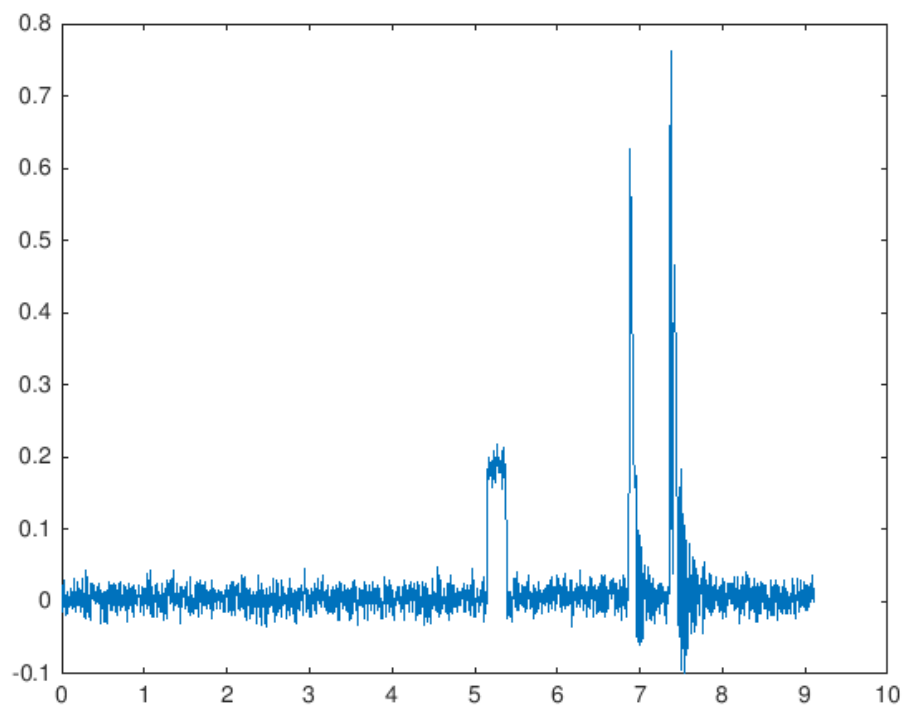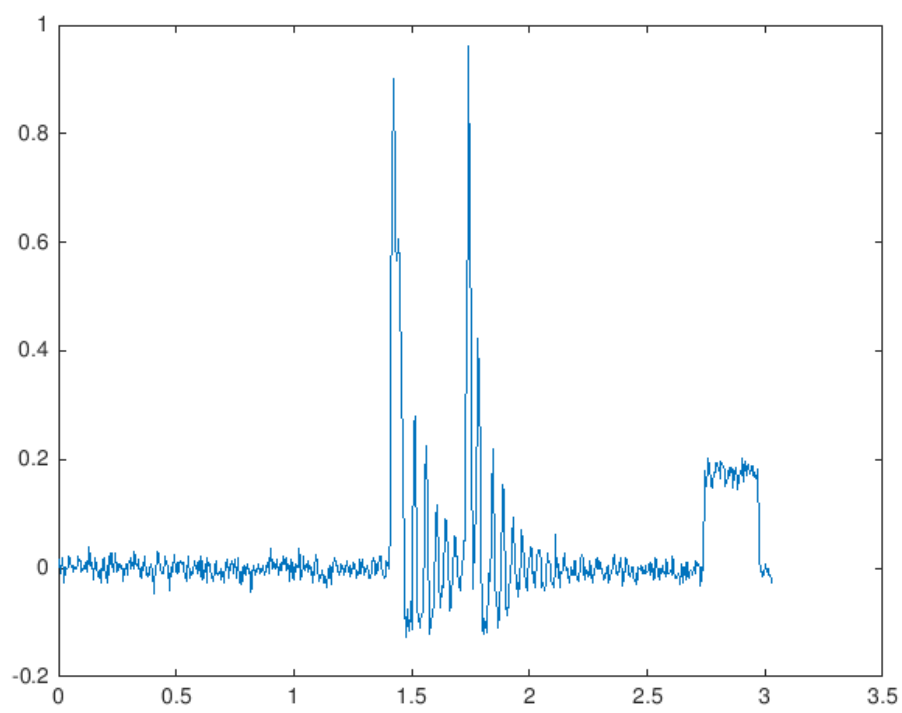

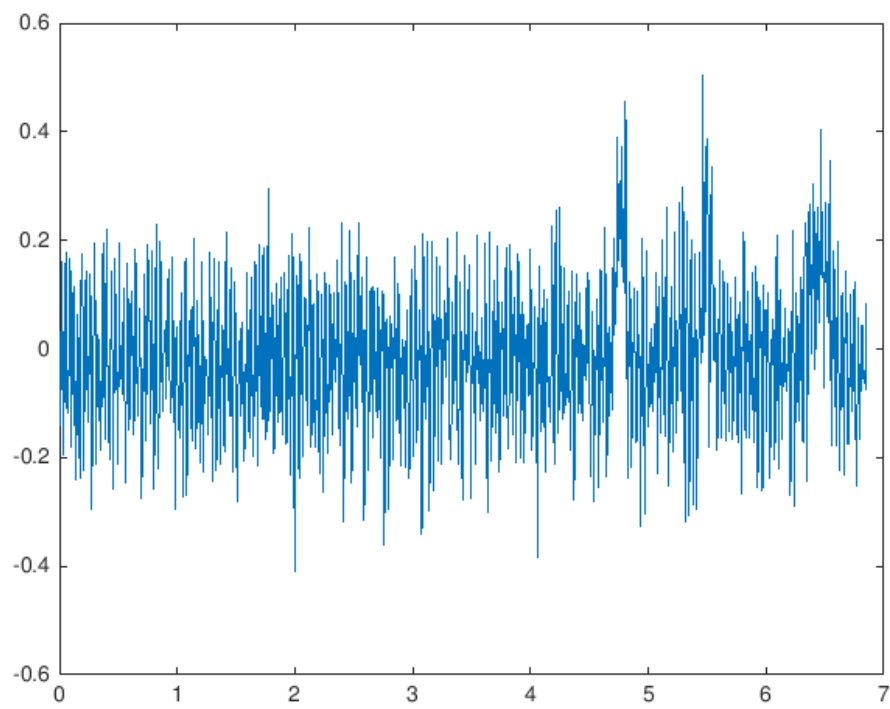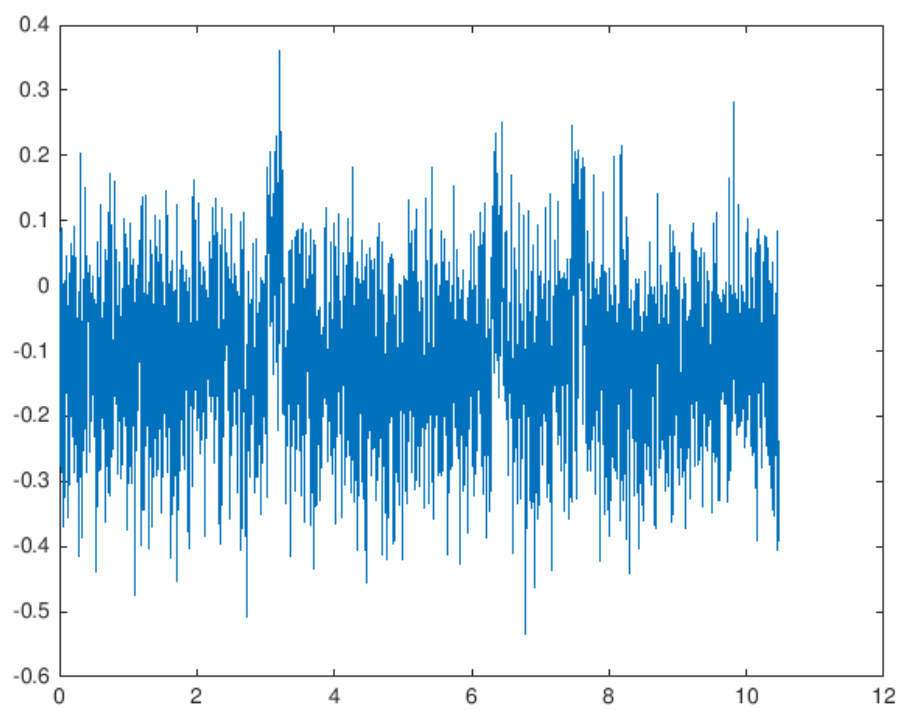(a) Test 1.1
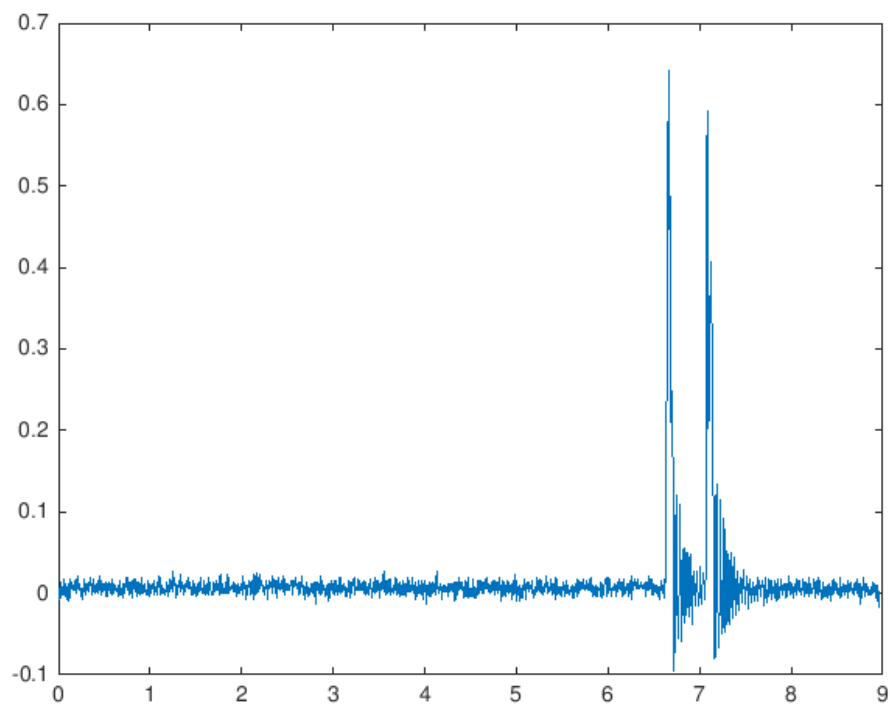
(b) Test 1.2
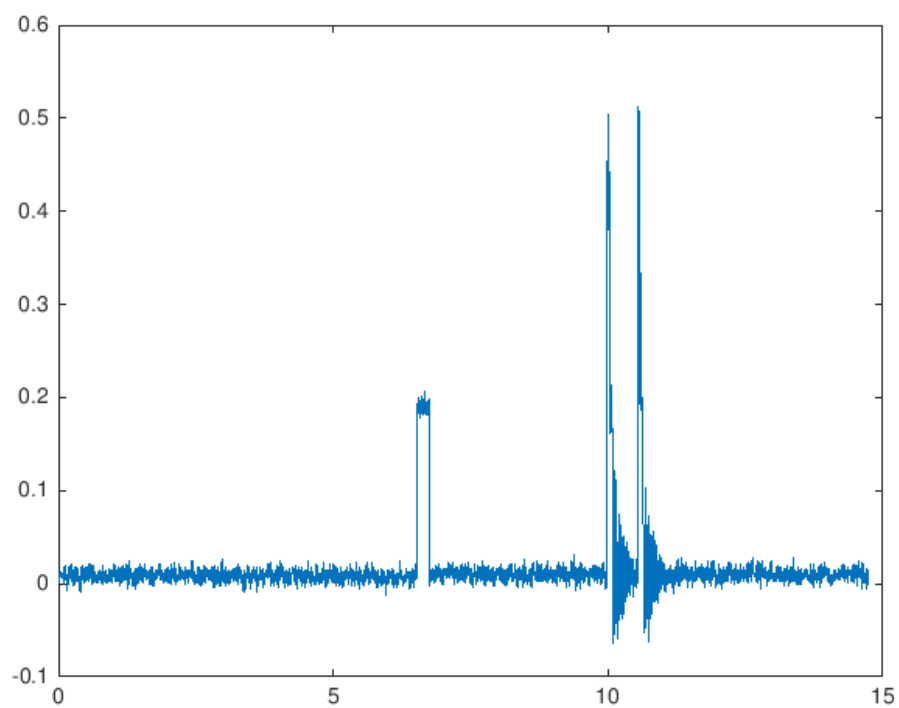
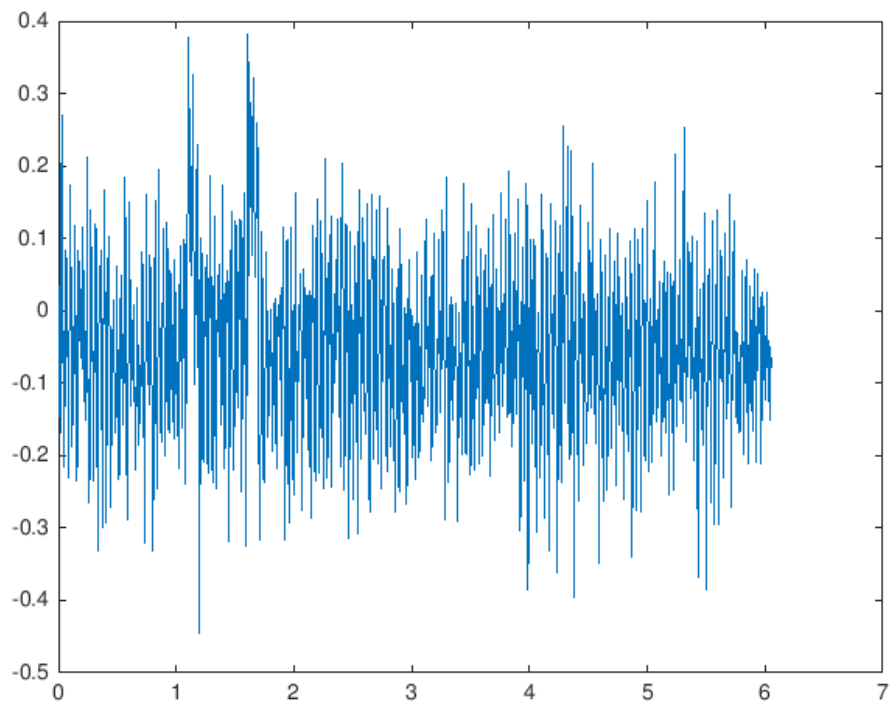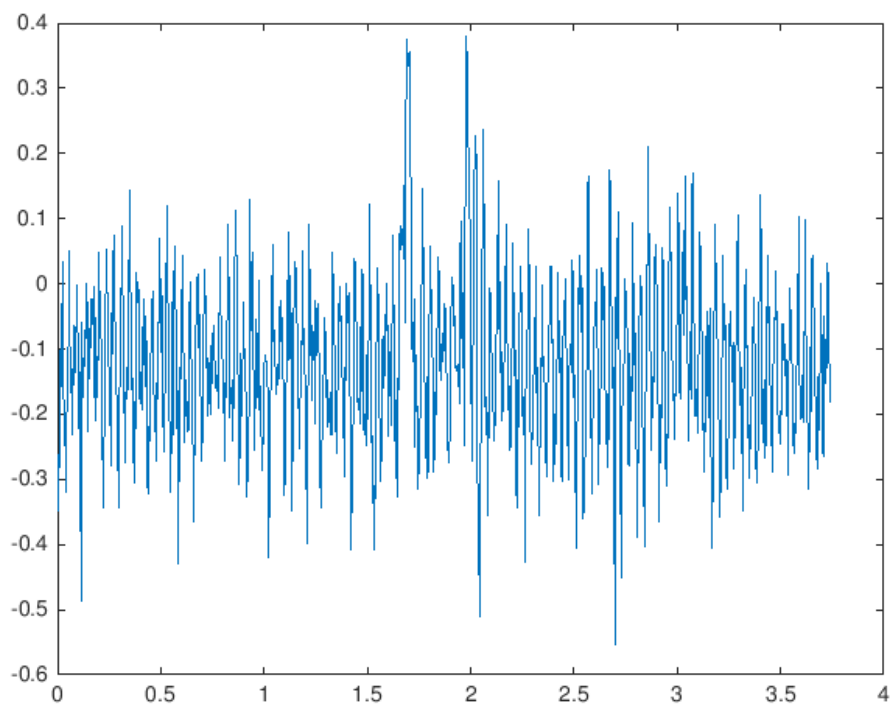(c) Test 1.3

(d) Test 1.4

(e) Test 1.5

(f) Test 1.6

(g) Test 1.7

(h) Test 2.1

(i) Test 2.2

(j) Test 2.3

(k) Test 2.4
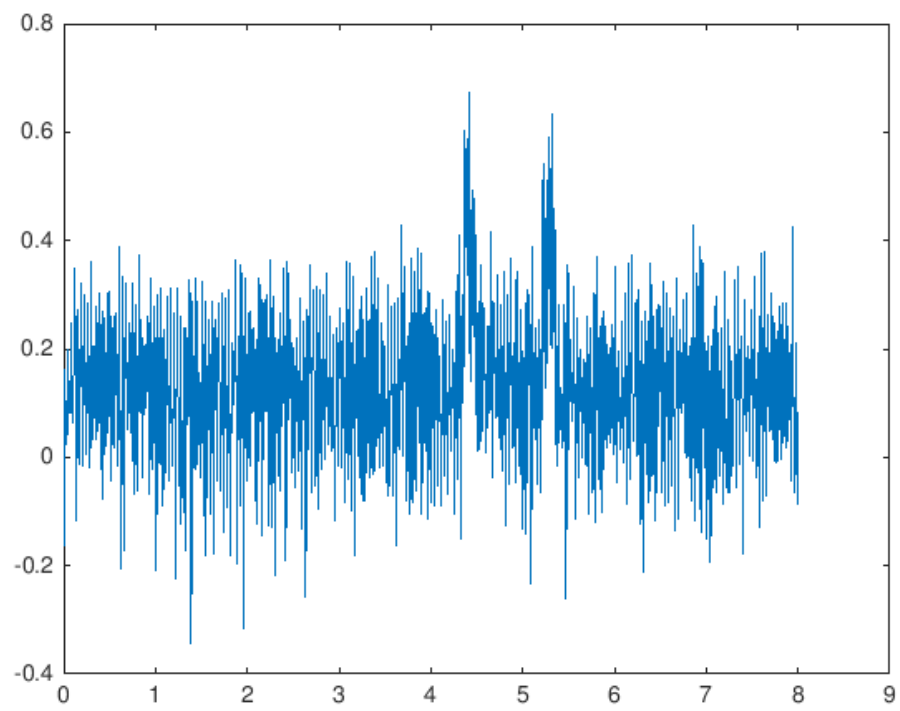
(l) Test 2.5
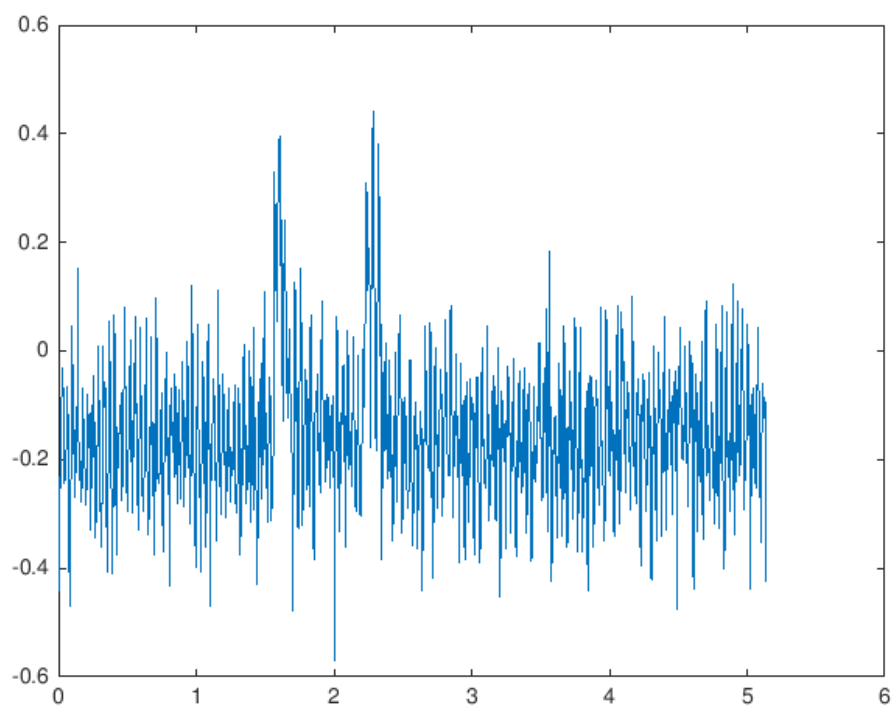
(m) Test 2.6
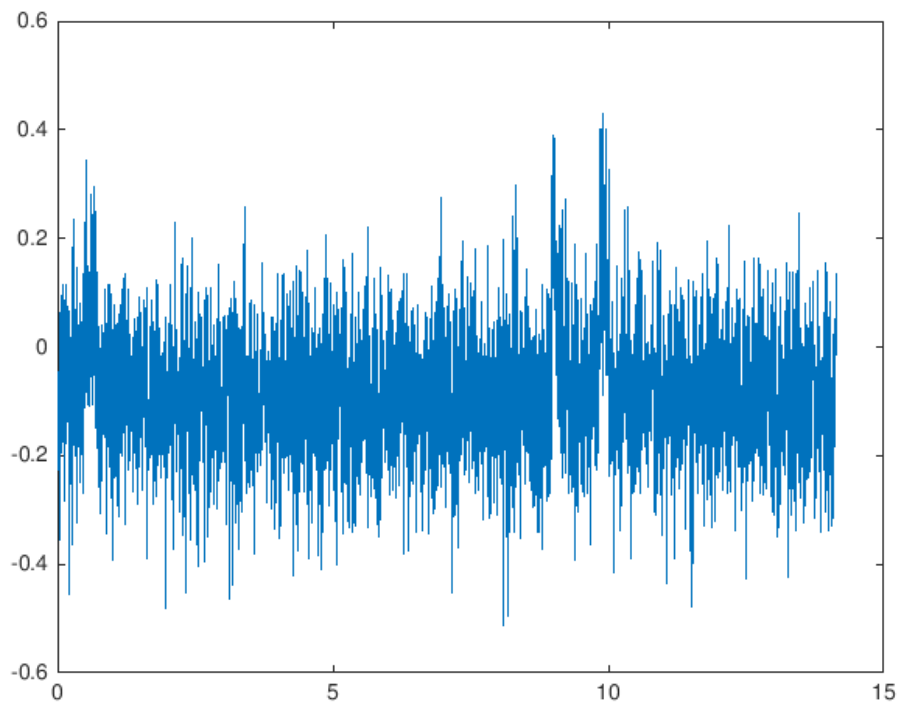
(n) Test 2.7
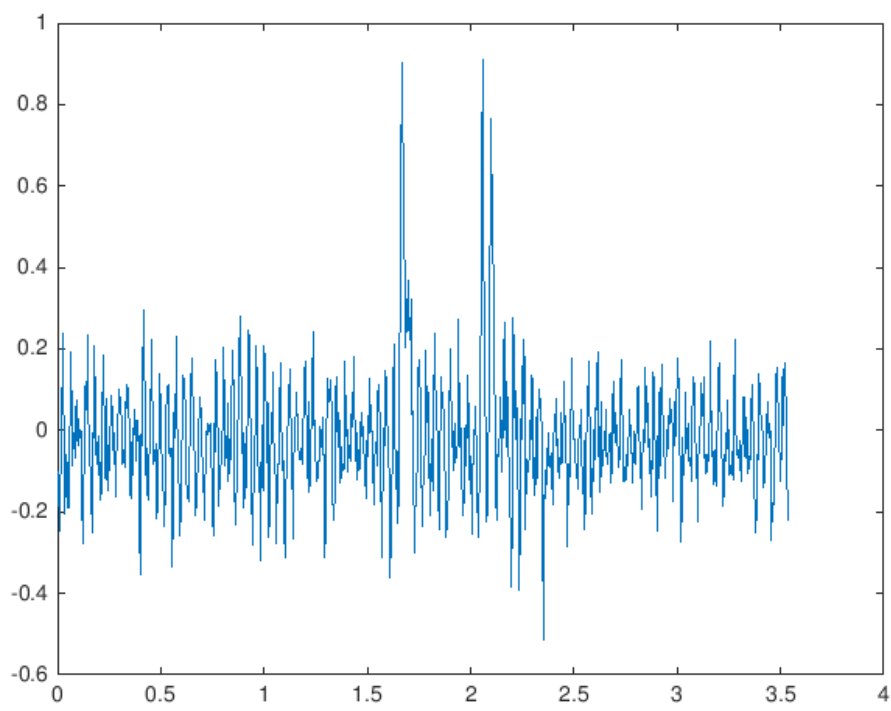
(o) Test 2.8
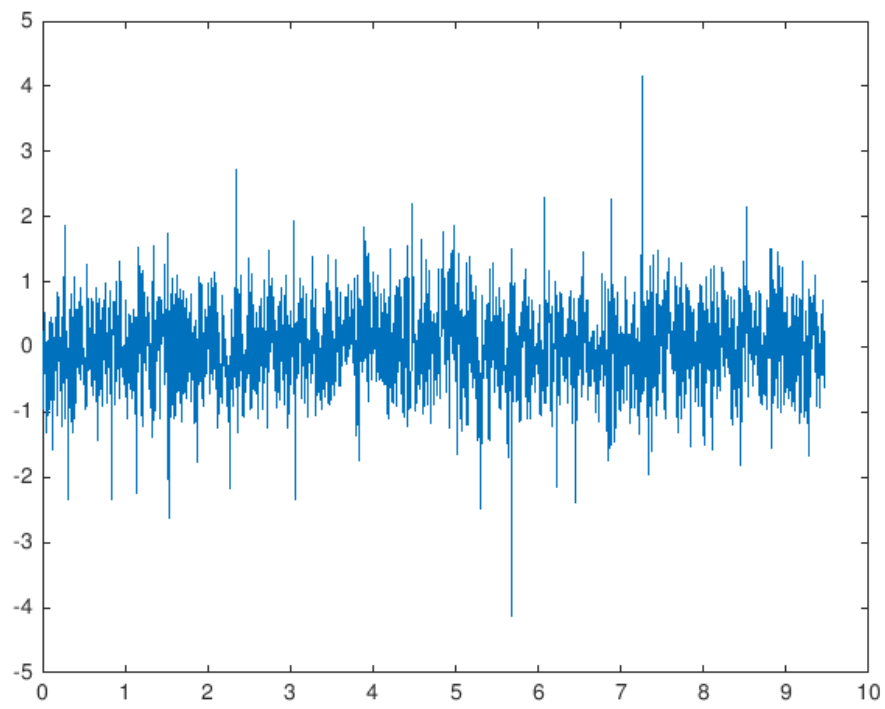
(p) Test 3.1
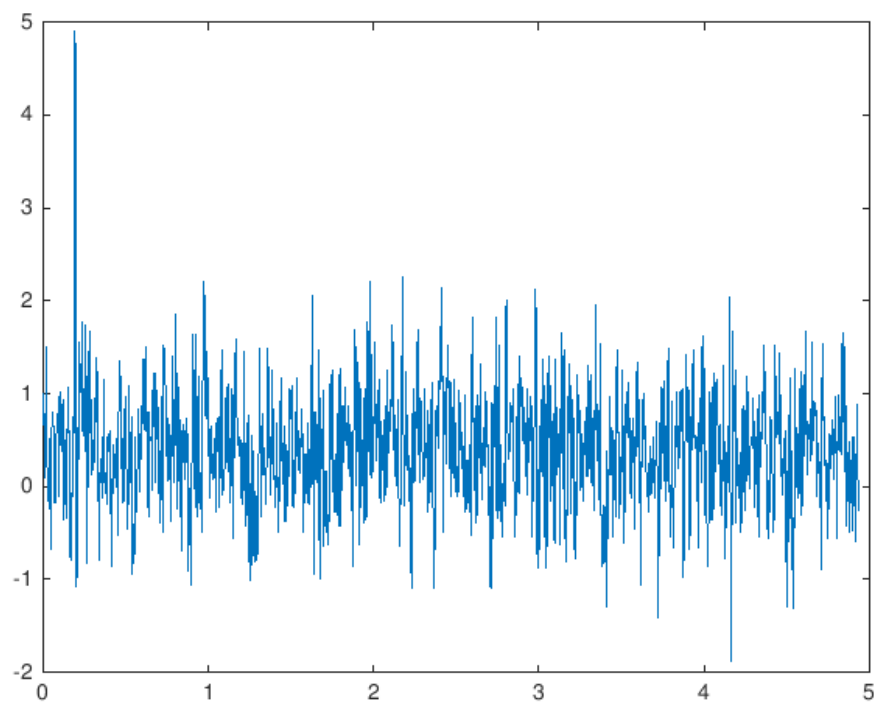
(q) Test 3.2
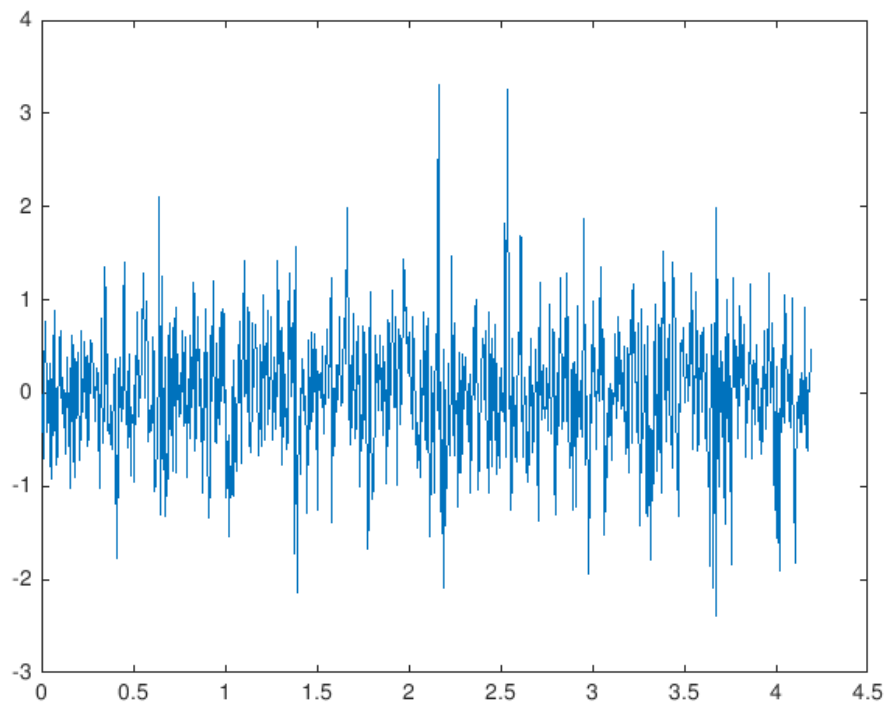
(r) Test 3.3
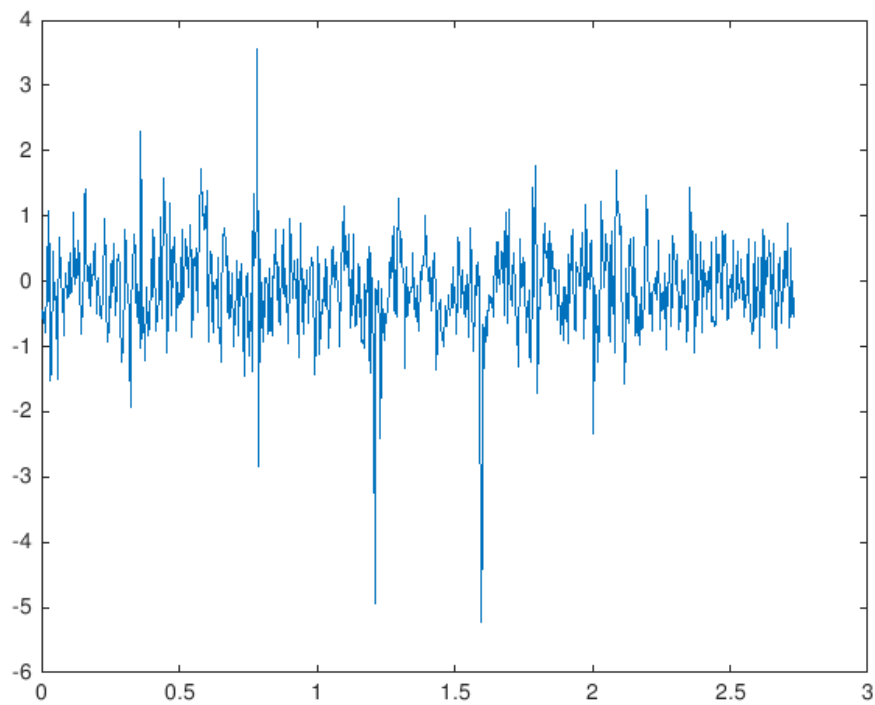
(s) Test 3.4

Figure B.1: Plotted load cell raw data, [kN] vs. [s].

Appendix C

Principle Component Regression Analysis of Test Data

Project Administrator Eirik Furuholmen performed principle component regression analysis of the physical testing data presented in 4.3, to evaluate the strength of the data in predicting load values based on speed and inclination. Analysis was performed on two data sets, one consisting of speed, inclination and front wheel load for tests 1.1 to 1.7, and one consisting of the same factors for tests 2.3 to 2.6 and 2.8. Based on the data, the software creates a prediction function. To evaluate the strength of the data, Eirik attempted to predict values for the tests that were actually preformed, to assess the accuracy of the predictions.

By observing the figures presented in table C.1, it appears so that the data from the first day of testing provides a much better basis for predictions than that of the second day of testing. This is as expected, considering the amount of signal noise experienced in the second day of testing, and the apparent lack of trends observed in the visual presentation of the data (4.6).

Test	Ramp inclination	Speed	Predicted front wheel load	Actual front wheel load	Percentage deviation
1.1	0.0 °	1.5 m/s	0.65 kN	0.78 kN	17.2%
1.2	3.8 °	3.7 m/s	1.21 kN	1.07 kN	12.9%
1.3	3.8 °	2.8 m/s	1.06 kN	1.05 kN	0.87%
1.4	3.8 °	5.4 m/s	1.49 kN	1.37 kN	8.88%
1.5	7.7 °	1.1 m/s	0.98 kN	0.84 kN	16.2%
1.6	7.7 °	3.1 m/s	1.31 kN	1.39 kN	5.93%
1.7	7.7 °	4.7 m/s	1.57 kN	1.76 kN	10.6%
				Avg:	10.4%
2.3	3.8 °	3.0 m/s	0.92 kN	1.22 kN	24.6%
2.4	3.8 °	4.5 m/s	0.90 kN	0.96 kN	6.08%
2.5	7.7 °	1.7 m/s	1.75 kN	1.85 kN	5.30%
2.6	7.7 °	2.2 m/s	1.75 kN	0.92 kN	89.8%
2.8	11 °	3.9 m/s	2.55 kN	2.92 kN	12.6%
				Avg:	27.7%

Table C.1: Predicted vs. real loads on front wheel based on regression.

Appendix D

Risk Assessment Form

Please note that the attached risk assessment is written in Norwegian.

ID	30947		Status	Dato
Risikoområde	Risikovurdering: Helse, miljø og sikkerhet (HMS)		Opprettet	11.12.2018
Opprettet av	Lars Røed Ramstad		Vurdering startet	11.12.2018
Ansvarlig	Lars Røed Ramstad		Tiltak besluttet	
			Avsluttet	11.12.2018

Risikovurdering:
Risikovurdering Prosjektarbeid

Gyldig i perioden:
9/1/2018 - 6/11/2019

Sted:
Trondheim

Mål / hensikt
Hensikten med denne vurderingen er å avdekke potensiell risiko involvert med gjenomføringen av forfatterens prosjekt/master arbeid, og om nødvendig inverksette tiltak for å begrense nevnte risiko.

Bakgrunn
Risikovurderingen utføre i henhold til standard prosedyre for eksperimentelt arbeid ved NTNU.

Beskrivelse og avgrensninger
Aktiviteter inkluderer bruk av verktøy ved MTP's realiseringlab, inkludert både håndverktøy og maskiner omfatet av MTP's krav til HMS opplæring. I tillegg inkluderer vurderingen risiko ved testing av komponenter og kjøretøy, både i og utenfor labben.mponent testing in- and outside of the workshop.

Forutsetninger, antakelser og forenklinger
Assumptions are made that machines and equipment at the lab are properly maintained and functional, and that other users in the workshop are trained in and follow the HSE guidelines given by MTP.
Det antas at maskiner og utstyr ved realiseringslabben er godt vedlikeholdt og at andre brukere ved labben har og benytter seg av HMS opplæringen gitt ved MTP.

Vedlegg
[Ingen registreringer]

Referanser
[Ingen registreringer]

Oppsummering, resultat og endelig vurdering

I oppsummeringen presenteres en oversikt over farer og uønskede hendelser, samt resultat for det enkelte konsekvensområdet.

Farekilde: **Maskinverktøy**

Uønsket hendelse: **Små kutt**

Konsekvensområde: Helse   Risiko før tiltak: 🟢   Risiko etter tiltak: ⚪

Uønsket hendelse: **Klemskader**

Konsekvensområde: Helse   Risiko før tiltak: 🟡   Risiko etter tiltak: ⚪

Uønsket hendelse: **Sponsprut i øyne**

Konsekvensområde: Helse   Risiko før tiltak: 🟡   Risiko etter tiltak: ⚪

Farekilde: **Bruk av tungt utstyr og materialer**

Uønsket hendelse: **Klemming av lemmer under tung gjenstand**

Konsekvensområde: Helse   Risiko før tiltak: 🟢   Risiko etter tiltak: ⚪

Farekilde: **Bruk av sveiseapparat/plasmabrenner o.l.**

Uønsket hendelse: **Brannskade**

Konsekvensområde: Helse   Risiko før tiltak: 🟢   Risiko etter tiltak: ⚪

Farekilde: **Testing av kjøretøy**

Uønsket hendelse: **Kollisjon**

Konsekvensområde: Helse   Risiko før tiltak: 🟢   Risiko etter tiltak: ⚪
                       Ytre miljø   Risiko før tiltak: 🟢   Risiko etter tiltak: ⚪
                       Materielle verdier   Risiko før tiltak: 🟡   Risiko etter tiltak: ⚪

Endelig vurdering

Norges teknisk-naturvitenskapelige universitet (NTNU)   **Utskriftsdato:**   **Utskrift foretatt av:**   **Side:**

Unntatt offentlighet jf. Offentlighetsloven § 14   11.12.2018   Lars Røed Ramstad   2/13

Det eksisterer som alltid risiko for helse ved bruk av kraftige verkstedmaskiner. Forhåndstiltak som aktsom bruk og korrekt anvendelse av verneutstyr kan ikke fullstendig utelukke disse, og fortløpende vurderinger av risiko må derfor utføres ved utførelse av ethvert arbeid.

Ettersom prosjektet kun konstruerer lette kjøretøy begrenset til svært lav hastighet er fare for helse og ytre miljø lav. Eget materielt utstyr kan derimot lett skades, og ved ethvert eksperiment bør nytteverdien vurderes opp mot risikoen for slike skader.

Involverte enheter og personer

En risikovurdering kan gjelde for en, eller flere enheter i organisasjonen. Denne oversikten presenterer involverte enheter og personell for gjeldende risikovurdering.

Enhet /-er risikovurderingen omfatter

 - NTNU

Deltakere

 Lesere

[Ingen registreringer]

Andre involverte/interessenter

[Ingen registreringer]

Følgende akseptkriterier er besluttet for risikoområdet Risikovurdering: Helse, miljø og sikkerhet (HMS):

Helse	**Materielle verdier**	**Omdømme**	**Ytre miljø**

Oversikt over eksisterende, relevante tiltak som er hensyntatt i risikovurderingen

I tabellen under presenteres eksisterende tiltak som er hensyntatt ved vurdering av sannsynlighet og konsekvens for aktuelle uønskede hendelser.

Farekilde	Uønsket hendelse	Tiltak hensyntatt ved vurdering
Maskinverktøy	Små kutt	
	Klemskader	Bruk av tettsittende tøy og fravær av hansker, løse tråder o.l.
	Klemskader	Bruk av tettsittende tøy, samt fravær av hansker
	Sponsprut i øyne	Bruk av vernebriller
Bruk av tungt utstyr og materialer	Klemming av lemmer under tung gjenstand	Bruk av vernesko med ståltupp
Bruk av sveiseapparat/plasmabrenner o.l.	Brannskade	Bruk av sveisefrakk og maske
Testing av kjøretøy	Kollisjon	Ikke utfør testing på traffikkerte områder
	Kollisjon	Benytt fempunkts setebelte i bilen
	Kollisjon	Ikke utfør testing på traffikkerte områder
	Kollisjon	Benytt fempunkts setebelte i bilen

Eksisterende og relevante tiltak med beskrivelse:

Bruk av vernebriller

-

Bruk av tettsittende tøy, samt fravær av hansker

-

Bruk av vernesko med ståltupp

-

Ikke utfør testing på traffikkerte områder

-

Benytt fempunkts setebelte i bilen

-

Bruk av sveisefrakk og maske

-

Risikoanalyse med vurdering av sannsynlighet og konsekvens

I denne delen av rapporten presenteres detaljer dokumentasjon av de farer, uønskede hendelser og årsaker som er vurdert. Innledningsvis oppsummeres farer med tilhørende uønskede hendelser som er tatt med i vurderingen.

Følgende farer og uønskede hendelser er vurdert i denne risikovurderingen:

- **Maskinverktøy**
    - Små kutt
    - Klemskader
    - Sponsprut i øyne
- **Bruk av tungt utstyr og materialer**
    - Klemming av lemmer under tung gjenstand
- **Bruk av sveiseapparat/plasmabrenner o.l.**
    - Brannskade
- **Testing av kjøretøy**
    - Kollisjon

Detaljert oversikt over farekilder og uønskede hendelser:

Farekilde: Maskinverktøy

Uønsket hendelse: Små kutt

- -

Sannsynlighet for hendelsen (felles for alle konsekvensområder):   **Sannsynlig (3)**

    Kommentar:
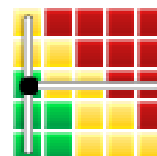   [Ingen registreringer]

Konsekvensområde: Helse   *Risiko:*

    Vurdert konsekvens: **Liten (1)**

        Kommentar: [Ingen registreringer]

Uønsket hendelse: Klemskader

- -

Sannsynlighet for hendelsen (felles for alle konsekvensområder):   **Svært lite sannsynlig (1)**

    Kommentar:
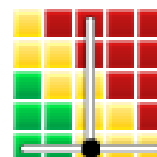   [Ingen registreringer]

Konsekvensområde: Helse   *Risiko:*

    Vurdert konsekvens: **Stor (3)**

        Kommentar: [Ingen registreringer]

Norges teknisk-naturvitenskapelige universitet (NTNU)

Unntatt offentlighet jf. Offentlighetsloven § 14

Utskriftsdato:
11.12.2018

Utskrift foretatt av:
Lars Røed Ramstad

Side:
7/13

Uønsket hendelse: Sponsprut i øyne
- -

Sannsynlighet for hendelsen (felles for alle konsekvensområder):   **Svært lite sannsynlig (1)**

      Kommentar:

      [Ingen registreringer]

Konsekvensområde: Helse

    Vurdert konsekvens: **Svært stor (4)**

      Kommentar: [Ingen registreringer]

Risiko:

Farekilde: Bruk av tungt utstyr og materialer

Uønsket hendelse: Klemming av lemmer under tung gjenstand

Sannsynlighet for hendelsen (felles for alle konsekvensområder): **Lite sannsynlig (2)**

Kommentar:
[Ingen registreringer]

Konsekvensområde: Helse

Vurdert konsekvens: **Middels (2)**

Kommentar: [Ingen registreringer]

Risiko:

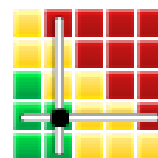**Farekilde: Bruk av sveiseapparat/plasmabrenner o.l.**

Uønsket hendelse: Brannskade

Sannsynlighet for hendelsen (felles for alle konsekvensområder): **Lite sannsynlig (2)**

    Kommentar:

    [Ingen registreringer]

Konsekvensområde: Helse

    Vurdert konsekvens: **Middels (2)**

        Kommentar: [Ingen registreringer]

Risiko:

Farekilde: Testing av kjøretøy

Uønsket hendelse: Kollisjon

Sannsynlighet for hendelsen (felles for alle konsekvensområder): **Sannsynlig (3)**
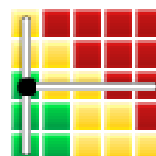
    Kommentar:
    [Ingen registreringer]

Konsekvensområde: Helse

    Vurdert konsekvens: **Liten (1)**

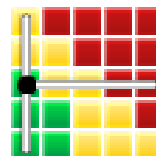   *Kommentar:* [Ingen registreringer]

Risiko:

Konsekvensområde: Ytre miljø

    Vurdert konsekvens: **Liten (1)**

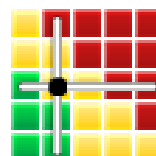   *Kommentar:* [Ingen registreringer]

Risiko:

Konsekvensområde: Materielle verdier

    Vurdert konsekvens: **Middels (2)**

        Kommentar: [Ingen registreringer]

Risiko:

Norges teknisk-naturvitenskapelige universitet (NTNU)

Unntatt offentlighet jf. Offentlighetsloven § 14

Utskriftsdato:
11.12.2018

Utskrift foretatt av:
Lars Røed Ramstad

Side:
11/13

Oversikt over besluttede risikoreduserende tiltak:

Under presenteres en oversikt over risikoreduserende tiltak som skal bidra til å reduseres sannsynlighet og/eller konsekvens for uønskede hendelser.

Detaljert oversikt over besluttede risikoreduserende tiltak med beskrivelse:

Detaljert oversikt over vurdert risiko for hver farekilde/uønsket hendelse før og etter besluttede tiltak

Bibliography

[1] Shell. *Shell Eco–Marathon 2019 Official Rules*. 2018.

[2] Shell. *Shell Eco–Marathon 2018 Official Rules*. 2018.

[3] Richard Stone and Jeffrey K. Ball. *Automotive Engineering Fundamentals*. SAE International, 2004.

[4] Department of the Army. *TM 9-8000 Principles of Automotive Vehicles,*. 1985.

[5] William H. Crouse. *Automotive Mechanics*. McGraw-Hill, 1965.

[6] Pei-Shi Huang and Alfred Pruckner. *Steer by Wire, in: Steering Handbook*. 2017.

[7] Thomas D. Gillespie. *Fundamentals of Vehicle Dynamics*. SAE International, 1992.

[8] Sadjyot Biswal, Aravind Prasanth, M S Dhiraj Sakhamuri and Shaurya Selhi. Design and Optimization of the Steering System of a Formula SAE Car Using Solidworks and Lotus Shark , 2016.

[9] J. Bernard D. Isler P. Kobler F. Kolb N. Weidmann L. Guzella J.J. Santin, C.H. Onder. *The World's Most Fuel Efficient Vehicle - Design and Development of PAC-car II*. vdf, 2007.

[10] Hans Pacejka. *Tire and Vehicle Dynamics*. 2012.

[11] Richard G. Budynas and J. Keith Nisbett. *Shigley's Mechanical Engineering Design*. McGraw-Hill, 2011.

[12] Brian M. Kennedy, Durward K. Sobek and Michael N. Kennedy. Reducing Rework by Applying Set-Based Practices Early in the Systems Engineering Process, 2013.

[13] Stepahnie Houde et al. Handbook of Human-Computer Interaction, 1997.

[14] Sivert Røed Hatletveit. *Development of a Energy Efficient Powertrain*. 2018.

Websites

[15] DNV GL Fuel Fighter. `https://www.fuelfighter.no/`. [Online; accessed 13-November-2018].

[16] Shell. Shell Eco–Marathon. `https://www.shell.com/energy-and-innovation/shell-ecomarathon.html`. [Online; accessed 13-November-2018].

[17] "Bromskloss". Ackermann. `https://commons.wikimedia.org/wiki/File:Ackermann.svg`, 2006. [Online; accessed 14-November-2018].

[18] Helmut Ormestad. Friskjon. `https://snl.no/friksjon`. [Online; accessed 23-November-2018].

[19] AEP Transducers. C8S. `http://www.aeptransducers.com/force-transducers/100-c8s.html`. [Online; accessed 07-December-2018].

[20] HBM. QuantumX. `https://www.hbm.com/en/2128/quantumx-compact-universal-data-acquisition-system/`. [Online; accessed 07-December-2018].